Sedimentology of a transgressive middle-upper Miocene succession filling a tectonically confined, current dominated seaway (the Logudoro Basin, northern Sardinia, Italy)

Donatella Telesca [a], Sergio G. Longhitano [a,*], Marco Pistis [b], Vincenzo Pascucci [c], Marcello Tropeano [d], Luisa Sabato [d,e]

[a] *Department of Sciences, University of Basilicata, V.le Ateneo lucano 10, 85100 Potenza, Italy*
[b] *Department of Chemical and Geological Sciences, University of Cagliari, Italy*
[c] *Department of Architecture, Design and Urbanistic, University of Sassari, I-07041 Alghero, Italy*
[d] *Dipartimento di Scienze della Terra e Geoambientali, University of Bari, Italy*
[e] *Dipartimento di Biologia, University of Bari, Italy*
*corresponding

Abstract

The sedimentary dynamics of modern current dominated seaways are well known, based on the monitoring of movement of large sand bodies over short time-scales and the geophysical reconstruction of millennial time-scale processes from recent subsurface successions. Analogues from the ancient record are less common and the longer-term (geological time-scale) sedimentary dynamics of such systems is still not properly assessed or understood. In this work, we review the interpretation of a Serravallian sand-rich stratigraphic interval (namely, the 'Sabbie di Florinas' Fm), variously exposed in the Logudoro Basin, a Miocene 10 km-wide and 20 km-long, tectonically-confined extensional depression, developed as a segment of the wider Sardinian Graben System, Italy. The basin includes three main depositional sequences separated by regional-scale unconformities and encompassing the middle Burdigalian to the late Messinian. The intermediate sequence, Serravallian-Tortonian in age, is the one that records the onset of the marine connection between two small basins (i.e., the Logudoro to the south and the Porto Torres to the north), which were previously isolated, resembling endorheic conditions. The oceanographic opening of a seaway, at the beginning of a regional-scale marine transgression, is firstly sug- gested by facies indicating a strong current reworking of sediment transiting along submerged deltaic platforms, where cross-bedded vertically stacked m-thick sandstone intervals prevail. These deposits correspond with large-scale cross-bedded sand bodies in the axial part of the seaway, where energetic currents promoted the mi- gration of bedforms (i.e., bars and subaqueous dunes). The overlying deposits, accumulated during a late stage of transgression, show an increased maturity of textural and grain size features and exhibit herringbone cross bed- ding, reactivation surfaces and lamina bundles indicative of a clear tidal signature. At this stage, the seaway experienced a more mature oceanographic setting, governed by bi-directional and rotatory current patterns oriented roughly parallel to the elongation axis. Carbonate-rich large-scale bedforms (i.e., ridges) developed dur- ing this late stage of open-marine circulation, inferring possible conditions for sediment starvation in the basin. This work reconstructs the depositional scenario of a segment of the wider Sardinian Seaway, which intermit- tently connected isolated basins along the Sardinian Graben System. Moreover, the data discussed in this paper help in unravelling the complex sedimentary dynamics of ancient seaways and highlight their relevance for even more accurate palaeogeographic reconstructions.

1. Introduction

Depositional models for modern marine settings, where currents play a key role in sedimentary dynamics, are recently increasing in number and quality of data, thanks to improved techniques of investigation (e.g., Belderson et al., 1982; Saito et al., 1998; Davis and Balson, 1992; Harris et al., 1995; Viana et al., 1998; Reynaud et al., 1999; Berné et al., 2002; Lim et al., 2006; Park et al., 2006; Suter, 2006; Reynaud and Dalrymple, 2012; Li et al., 2014; Daniell, 2015; Gupta et al., 2017). How- ever, reconstructions based on ancient current-dominated settings are still relegated to a limited number of examples, or mostly focused on the characterisation of sand-prone facies due to their higher economic relevance (e.g., Allen and Homewood, 1984; Swift and Rice, 1984; Gaynor and Swift, 1988; Surlyk and Noe-Nygaard, 1991; Mellere and Steel, 1996; Anastas et al., 1997, 2006; Braga et al., 2010; Leva-López et al., 2016; Capella et al., 2017). This work aims at contributing to fill this gap by presenting a field-based case study reconstructing the sediment dynamics of a segment of a tectonically-controlled seaway, which underwent a phase of marine transgression during the Serravallian. The study area of the present work corresponds with the Logudoro Basin, Sardinia, Italy (Fig. 1A). It is a 10 km-wide and 20 km-long half- graben, which was a northern segment of the larger Sardinian Graben System active during the Miocene (Fig. 1A, B). Its basin-fill succession includes three regional-scale depositional sequences, consisting of conti- nental, shallow-marine to deep-sea siliciclastic deposits, associated with localised bioclastic intervals (Mazzei and Oggiano, 1990; Martini et al., 1992; Funedda et al., 2000, 2003) (Fig. 1B).

The Sardinian Graben System developed with an E-W-stretching extension in a back-arc setting during the Miocene (Casula et al., 2001) (Fig. 1C, D). Owing to a polyphase tectonic evolution, coalescent small endorheic basins along the main extensional lineaments became intermittently connected during repeated major Miocene transgres- sions. Consequently, the graben system turned into a marine seaway (namely the 'Sardinian Seaway'; Longhitano et al., 2017) (Fig. 1D), being progressively filled by continental and marine, extra-basinal clastics and intra-basinal carbonates. The sedimentary basin-fill succession is today partially exposed along the eastern side of the Campidano Basin, a Plio-Quaternary extensional depression structurally superimposed on to the Miocene graben (Sowerbutts and Underhill, 1998). Portions of the graben today expose sedimentary deposits exhibiting diagnostic motifs of large-scale cross stratification, which have been preliminarily considered as evidence for a current- dominated setting (Reynaud et al., 2013; Longhitano et al., 2017).

The present study reviews the environmental interpretation of a sand-rich Serravallian interval belonging to the intermediate sedimen- tary sequence, namely the 'Sabbie di Florinas' Fm, based on detailed facies analysis of outcrops exposed in this part of the Sardinia island (Fig. 2A, B). This formation records a stage of opening of the Logudoro Basin when it became part of a larger marine seaway, possibly domi- nated by shore-parallel propagating marine currents. The results achieved with the present work aim at improving the reconstruction of the Sardinian Seaway in the palaeo-oceanographic setting of the western Mediterranean during the Miocene, and to make some progress in the knowledge of ancient current-dominated straits and seaways.

2. Current-dominated shallow-marine environments: state of the art and uncertainties

Subaqueous currents play an important role in influencing shallow- and deep-water marine environments, governing net-gross sediment distribution and sedimentary processes (Johnson and Baldwin, 1996; Stow et al., 2009; Hernández-Molina et al., 2011; Reynaud and Dalrymple, 2012). Models for these current-dominated environments refer to specific oceanographic conditions and predict sediment distribution patterns according to a general trend of current velocity deple- tion. As the flow strength decreases, as well as its transport capacity, sediments reduce in grain size, being organised into a specific bedform continuum in a down-current direction (Belderson and Stride, 1966; Belderson et al., 1982; Grochowski et al., 1993; Stow et al., 2009; Mitchell et al., 2013).

Current-dominated environments have benefited from many detailed studies, thanks to improving technology and focused on Recent-to-Present settings. These investigations document subaque- ous areas lying under the dominant effect of currents and forming a variety of bedforms, and emphasize the importance of sediment reworking and recycling during different stages of basin history (e.g., Berné et al., 1998; Hernández-Molina et al., 2016; Cattaneo et al., 2017).

Recent literature focused on either ancient or modern examples doc- uments that narrow, elongate basins are ideal loci for current amplifica- tion (Wells et al., 2010a, 2010b). Seaways and straits respond to such hydrodynamics by generating specific depositional zones and thus stratigraphic patterns (Longhitano, 2013; Longhitano and Chiarella, 2020). One of the main diagnostic features recognizable in ancient successions is the abundance of sand-rich deposits, which record areas of current high speed, whereas mud fractions accumulate in lower-energy reaches, lateral or distal with respect to the current main path- ways (Belderson et al., 1982; Dalrymple, 2019). Moreover, complexes of cross stratification with internal hierarchies of bounding surfaces and foresets, corresponding to extensive bedform fields in modern counterparts, are another stratigraphic element (e.g., Braga et al., 2010; Longhitano et al., 2012b, 2014). Nevertheless, case studies from the geological record are scarce, probably because current-dominated systems require extensive stratigraphic sections/outcrops and specific stratal exposures to well document large-scale geometrical features (e.g., Johnson and Baldwin, 1996). The identification of current- dominated settings in the rock record is also difficult because sedimen- tary processes can be influenced by flows of different strength and duration, resulting in complex sedimentary patterns or sediment trans- port routes. Likewise, the sedimentary signature of subaqueous currents may be masked by other oceanographic processes, such as waves and density currents, or after major episodes of sea floor erosion (Field, 1980; Swift and Rice, 1984; Gaynor and Swift, 1988; Surlyk and Noe-Nygaard, 1991; Swift et al., 1991). When currents dominate over other marine processes, such as waves, tides and density currents, classical depositional systems such as river deltas, shorefaces or shelves may preserve signatures that often depart from schematic models. In addi- tion, current-related processes may often cause uncertain sedimentary sinks because of the strong conditioning exerted by bottom roughness and basin-margin irregularities (e.g., Longhitano and Steel, 2016; Archer et al., 2019).

3. Geological setting of the Logudoro Basin

The Logudoro Basin was a NNW-trending, 10 km-wide and 20 km- long half-graben which hosted continental

to shallow-marine deposi- tion during repeated stages of sedimentation spanning the middle Burdigalian until the late Messinian (Funedda et al., 2000; Barca et al., 2005; Oudet et al., 2010) (Fig. 2A). The Logudoro Basin, as well as other coeval half-grabens (Sowerbutts and Underhill, 1998; Funedda et al., 2000, 2003), originated as a consequence of the counter- clockwise rotation of the Sardinian-Corsica block, in a general NE-SW- oriented extensional zone, occupying a back-arc regional-scale frame- work. From the Aquitanian to the late Burdigalian, this microplate drifting towards the central Mediterranean (Carminati et al., 2010) was affected by the eastward migration of the Alpine collisional front and the consequent opening of the Provençal Basin (e.g., Carmignani et al., 1995; Carminati and Doglioni, 2005) (Fig. 1C, D). The Logudoro Basin underwent phases of endorheic isolation, interrupted by episodic connections with adjacent marine areas to the north and south. These occasional openings were driven by the activation of E-W-striking transfer zones, which were also responsible for the establishment of open-marine settings (Gibbs, 1984; Bosworth, 1985; Carmignani et al., 1994, 1995; Faccenna et al., 2002; Oggiano et al., 2009) (Fig. 1B).

Three main fault systems controlled the sedimentation in the Logudoro Basin: (i) a middle-late Burdigalian, NNW-striking normal fault system (Thomas and Genneseaux, 1986; Oggiano, 1987), mainly controlling the western basin margin; (ii) a Serravallian, E-W-oriented strike-slip fault system (e.g., the Ittiri Fault) (Fig. 2A), which played an important role for the oceanographic interconnection of the Logudoro Basin to the north; and (iii) a Pliocene, N-S-trending normal fault system, along which intra-plate basaltic lava flows were emplaced (Funedda et al., 2000). During the Plio-Quaternary, many of these faults were reactivated, often interrupting the lateral continuity of the older sedimentary successions. The Miocene tectonic lineaments shaped the Logudoro Basin and adjacent depositional areas, generating a narrow-linear marine sector, triggering a general current-dominated oceanography (Telesca et al., 2016; Longhitano et al., 2017).

3.1. *The Logudoro Basin-fill succession*

The Logudoro Basin infill is up to 500 m thick and unconformably lies over the volcanic succession derived from Oligo-Miocene calcalkaline magmatism (Pietracaprina, 1962; Assorgia et al., 1988; Mazzei and Oggiano, 1990; Martini et al., 1992; Funedda et al., 2000, 2003; Oggiano et al., 2014) (Fig. 2B). The basin-fill succession, which is known to has been sourced by the adjacent NE-SW- trending Chilivani-Bechidda Basin (Oggiano et al., 1995; Funedda et al., 2000), encompasses the Miocene age starting from the middle Burdigalian (Fig. 1B) and has been subdivided into three deposi- tional sequences (Funedda et al., 2003; Donda et al., 2008).

The first sequence (?Middle Burdigalian-Langhian; Oggiano et al., 2014) includes terrestrial to marginal-marine conglomerates and sandstones, forming Gilbert-type deltas prograding into lacustrine deposits (Funedda et al., 2000). This lowermost interval, which records an endorheic setting, is transgressively overlain by condensed limestones and biocalcarenites passing upwards to shelf marlstones and siltstones and indicating the establishment of open-marine conditions (Fig. 2B). The overlying sequence boundary represents a basin-scale subaerial unconformity, which records a significant erosional *hiatus* comprising the late Langhian-early Serravallian (Mazzei and Oggiano, 1990; Martini et al., 1992; Funedda et al., 2000, 2003) (Fig. 2B).

The second depositional sequence includes the 'Sabbie di Florinas' Fm (Funedda et al., 2000), which is the focus of the present work (Fig. 2A, B). This succession has been ascribed to the Serravallian (Oggiano et al., 2014) and described as a series of stacked, 50 to 250 m-thick sandstone bodies exhibiting internal large-scale cross bedding (Martini et al., 1992). The first 40 m of the succession consist of cross-stratified sandstones, quartzitic

and granitoid pebble conglomer- ates and organic-rich fine sandstones indicating terrestrial deposition. Upwards, well-sorted quartz-feldspathic coarse-grained sandstones occur, showing large-scale cross-stratification (*SFa*; Fig. 2B), and including 1 to 20 m-thick biocalcarenitic intercalations that have been attributed to marginal- and shallow-marine settings (*SFb*; Fig. 2B) (Mazzei and Oggiano, 1990; Martini et al., 1992; Funedda et al., 2000, 2003). The 'Sabbie di Florinas' Fm is erosionally overlain by algae-rich limestones ascribed to the (?)Serravallian-early Messinian (Oggiano et al., 2014) and showing strata-scale cross bedding and large-scale clinoforms (Martini et al., 1992; Vigorito et al., 2006; Murru et al., 2015; Reuter et al., 2017) (Fig. 2B).

The younger depositional sequence crops out discontinuously in the Logudoro Basin and consists of up to 50 m-thick upper Messinian terrestrial claystones and conglomerates (Funedda et al., 2003). Extensive Plio-Quaternary basaltic plateaux lie unconformably on top of the Miocene deposits (Fig. 2B) and have preserved the underlying succession from excessive post-depositional subaerial erosion (Peccerillo, 2017).

4. Methods

This work has mainly been based on a first phase of geological mapping (Fig. 2A), integrated with the measurement of basin-scale cross sections, aiming at unravelling the lateral thickness changes of the 'Sabbie di Florinas' Fm and the stratigraphic relationships with under- and overlying units (Fig. 2C). During a second investigative phase, ten sedimentological logs have been acquired (Fig. 3) from quarries, road cuts and natural cliffs for a total vertical length of 336 m of logged succession, together with line drawings based on outcrop photomosaics and palaeocurrent measurements. Sedimentary facies have been described by taking into account grain size, lithology, internal structures, bedding style and fossil content, and are grouped into facies associations (Walker and James, 1992). The descriptive sedimentological terminology follows Harms et al. (1975, 1982) and Collinson et al. (2006). Sedimentary facies have been intended as the record of sedimentary environments belonging to specific systems (Harms et al., 1982; Walker, 1984). Microscope observations have provided textures, mineralogical features and the origin of biological elements indicative of a variety of energetic settings during sediment deposition.

5. Results

5.1. *Outcrop distribution of the Sabbie di Florinas Fm*

The study area is located in the northern sector of the Sardinian Gra- ben System (Sardinia, Italy) (Vardabasso, 1962; Cherchi and Montadert, 1982a, 1982b; Cherchi et al., 2008; Longhitano et al., 2015, 2017) (Fig. 1A), between the villages of Mores (to the south) and Florinas (to the north), south of Sassari (Fig. 1B). The 'Sabbie di Florinas' Fm crops out discontinuously in the study area due to post-depositional erosion and faulting (Fig. 2A). The succession also exhibits highly varying thick- nesses, from 30 to 250 m, because of the filling of an inherited topography deriving from incision of the underlying older sequence (Martini et al., 1992) (Fig. 2C).

The results deriving from the geological mapping and the measure- ment of geological cross sections, some of which are shown in Fig. 2C, indicate the 'Sabbie di Florinas' Fm lying confined between two main basement horsts, coinciding with the southwestern and northeastern basin margins. These areas are often block-faulted, although these lateral structures, presumably active during deposition of the Florinas sandstone, are not exposed continuously due to the superimposition of Quaternary lava flows. The 'Sabbie di Florinas' Fm occupies

the axial part of the Logudoro Basin and only locally it crops out near the margins (e.g., close to Ploaghe and Mores) (Fig. 2A, C). Based on the geological cross sections, one major depocentral zone can be recognised across the Logudoro Basin, located around the Mt. Pelao and Mt. Santo areas (Fig. 2A). Here, the 'Sabbie di Florinas' Fm reaches a maximum thickness of 250 m (see Fig. 2C), whereas it thins northwards showing a thickness of ca. 100 m in the Mt. Ruju area (see Fig. 2C). Marginal outcrops are well visible near Mores, Ploaghe and Florinas (Fig. 2A), where the formation shows thicknesses ranging between 30–40 m and 100 m (see Fig. 2C). This latter anomalous thickness for a marginal zone is inferred to be the effect of local control of active faulting. Southwards, there are no exposed outcrops of the 'Sabbie di Florinas' Fm because of the occurrence of older volcanic and volcaniclastic deposits, which are overlain by younger extensive basaltic plateaux (Fig. 1B). For this rea- son, this area is known to have underwent subaerial exposure during the Serravallian (Martini et al., 1992). Northwards, the 'Sabbie di Florinas' Fm continues until it disappears beneath the upper Miocene limestones (Oggiano et al., 2014).

5.2. *Facies analysis*

The sedimentological dataset documented for the 'Sabbie di Florinas' Fm identifies three main facies associations (Table 1). Their description follows a stratigraphic order from bottom to top and is separated from interpretations in the text.

5.3. *Facies association A: braid plain*

5.3.1. *Description*

This facies association represents the lowermost deposits exposed in the study area and erosionally lying on top of the older substrate. It crops out 1 to 2 km west from Mt. Santo, ranging from few meters to ca. 35 m in thickness (Fig. 3, Log #1). It is composed of three facies: A_1, A_2 and A_3 (Table 1).

5.3.2. *Facies A_1: braided channel and point bar deposits*

Facies A_1 consists of coarse-grained sandstone, pebbly sandstone and micro-conglomerate, forming a ca. 13 m-thick, composite foreset succession. This facies includes two vertically-stacked sub- facies (A_{1a} and A_{1b}) separated by an irregular erosional surface (Fig. 3, Log #1; Fig. 4A). The sub-facies A_{1a} consists of polymictic, quartzitic, granitoid pebbly sandstone and conglomerate, whose pebble- and cobble-size elements are angular to sub-rounded (Fig. 4B). Internally, sediments display 50–70 cm-thick individual cross-stratified sets, forming up to 2 m-thick indistinct co-sets (Fig. 4C). The overlying sub-facies A_{1b} is a texturally and mineralog- ically immature sandstone (Fig. 4C), rich in quartz and feldspar (≈50%), with a subordinate amount of biotite in a matrix (b15%) characterised by clay minerals. Internally, this sub-facies appears compound: 20–30 cm-thick amalgamated, normally graded planar- parallel stratified sets with erosional bases, form 1 to 3 m thick foreset units, which dip up to 25° SSW-wards and flattening upwards (Fig. 3, Log #1; Fig. 4C). Mudstone clasts are also randomly present in the uppermost part of this sub-facies (Fig. 3, Log #1). No macro- and microfauna have been recognised.

5.3.3. *Facies A_2: crevasse splay and floodplain deposits*

Facies A_2 lies 1–2 km laterally adjacent with the previous unit. It is exposed for a total thickness of ca. 13 m and includes two sub-facies (A_{2a} and A_{2b}). Sub-facies A_{2a} is made up of coarse-grained sandstone and subordinate siltstone, with rounded granules and pebbles, forming local planar-parallel laminae or appearing

scattered (Fig. 4D). This sand- stone sub-facies, which consists of arkose and minor volcanic lithics, is organised into vertically-stacked normally graded tabular beds (average thickness of 2 m), with erosional bases, forming a fining-upward succes- sion (Fig. 4D). Internally, strata contain indistinct low-angle cross strat- ification, sometimes highlighted by reddish-coloured coal fragments (Fig. 4E). Bioturbation is rarely present (BI = 1; Taylor and Goldring, 1993; Taylor et al., 2003) and consists of sporadic vertical burrows attributable to *Glossifungites* (Fig. 4E, F).

Sub-facies A_{2b} included in Facies A_2, erosionally overlies the deposits of Facies A_1 (Fig. 3, Log #1; Fig. 4A) and consists of greyish siltstone and subordinate fine-grained sandstone, characterised by 15 m-wide and 5 to 15 cm-thick lenticular intercalations, made up of sub-rounded poly- genic pebbles and cobbles (Fig. 4G, H). These interlayers are mainly concentrated at the base of individual beds, but rare isolated cobbles are scattered, where rare mudstone clasts, oriented parallel to the bedding, indicate the occurrence of indistinct internal cross stratification (Fig. 4I). This sub-facies reveals no fossiliferous content.

5.3.4. *Facies A_3: riverine ephemeral stream deposits*

Facies A_3 rests erosionally on both Facies A_2 and A_1 and reaches a maximum thickness of 6 m (Fig. 3, Log #1; Fig. 4A, C, G). It is a pebbly coarse-grained sandstone, also including siltstone in places, organised into tabular to lenticular up to 1 m-thick beds, normally graded and including cross stratification with north-trending foresets separated by internal erosional shallow scours (Fig. 4J, K). Locally coal laminae and mudstone clasts oriented parallel to the cross bedding are present (Fig. 4K, L). Concentrations of polymictic, sub-rounded pebble-size con- glomerates, a few cm thick, commonly aligned with internal bedding (i.e., at the bases of strata), also occur (Fig. 4J).

5.3.4.1. *Interpretation.* Facies association *A* is interpreted to record a segment of a fluvial braidplain, possibly feeding a wider alluvial area or a large alluvial fan system, including rivers and inter-channel areas (Cant, 1992; Collinson, 1996; Miall, 1996). Most likely, the constituting sediments were sourced from the western margin of the Logudoro Basin, thus indicating an alluvial braided system with an eastward drainage direction.

The lowermost Facies A_1 represents the traction-dominated deposition of sand-rich braided channels, containing laterally accret- ing active point bars/transverse bars (Allen, 1965; Collinson, 1996; Miall, 1996; Bridge, 1993, 2003). Lateral accretion is suggested based on the observation of: inclined strata sets, cross stratification, cross-stratified co-sets and internal erosional surfaces (Fig. 4A, C). The complex architecture of these bars is probably the result of entrenching channels active due to repeated flood events. This pro- cess arguably involved the same deposits and filled individual meandering braided channels, as a consequence of periodic phases of erosion, by-pass and deposition by river-flood tractive currents (Lanzoni, 2000a, 2000b; Bridge, 2003, 2006).

The differences in gravel content between the two sub-facies may reflect decreasing competence of the fluvial system through time or with distance from active channels. The erosional bases, associated with normal grading of the sandy A_{1b} sub-facies, document the deposition from currents with decreasing velocity and shallowing upwards due to progressive filling of the channels. The floating mud- stone clasts in the uppermost part of the succession are evidence of erosion by high-energy currents on previously-deposited muddy cohesive substrates, and the downcurrent accumulation of fragments by decreasing flow competence, which is typical of fluvial environments (e.g., Pye, 1994).

The sedimentary structures observed in Facies A_2 are indicative of deposition during the formation of crevasse splays (A_{2a}) and inter- channel floodplain areas (A_{2b}), which commonly characterise braided channels

during high-energy fluvial stages (Schumm, 1981; O'Brien and Wells, 1986; Collinson, 1996; Miall, 1996; Bridge, 2003, 2006). Transport occurs by overflow, after levee breaching, and resulting sediment-laden flood incursion on previous inter-channel areas. This type of current is strong enough to move dominantly sand and subordinately pebbles (Smith and Rogers, 1999; North and Davidson, 2012). In particular, basal erosion and the gravel concentrations in sub-facies A_{2a} are related to the initial stage of crevasse breaching, whereas normal grading is linked to progressive settling of suspended load (including mudstones clasts) as flow decelerates (Collinson, 1996; Miall, 1996; Smith and Rogers, 1999; Bridge, 2003, 2006). The plane-parallel oriented outsized clasts in the uppermost part of the beds results from bedload deposition from high-density flows and local traction carpets (Mutti and Nielsen, 1981; Postma et al., 1988). The presence of vege- tated areas close to the river channels is suggested by the abundant coal fragments and *Glossifungites* (Seilacher, 1967). This latter is indicative of compacted, semi-lithified substrates, characterised by very low sedimentation rates and reflects recolonization of firm-ground sub- strates (Pemberton and Frey, 1985; Uchman et al., 2000; Gingras et al., 2001; MacEachern et al., 1992, 2012; MacEachern and Burton, 2000). In the deposits of sub-facies A_{2b}, sedimentation occurred from settling of suspended load from flows inundating floodplain areas. Closer to river channels, local deposition of gravels records new flooding events. Cross-bedding, basal channel-lags and fining-upward trends documented for Facies A_3 are indicative of ephemeral streams excavated under lower energetic conditions when compared with the underlying channel-fills. The internal architectures record laterally accreting compound longitudinal bars (Allen, 1965; Bridge, 2003, 2006; Collinson
et al., 2006).

5.4. *Facies association B: submerged deltas*

5.4.1. *Description*

This facies association represents the most important stratigraphic interval in the study area in terms of areal extent and volume. This this facies association erosionally overlies the first depositional se- quence, as well as the previous facies association, although the basal boundary is not always well visible in outcrop.

Facies association *B* consists of two alternating facies: siliciclastic Fa- cies B_1 and mixed siliciclastic/bioclastic Facies B_2. This assemblage ranges in thickness from 40 m in the Ploaghe area, up to 350 m in the Mt. Santo area (Figs. 2C, 3).

Facies B_1: gravity-dominated, current-influenced delta-slope deposits Facies B_1 consists of sandstone-rich deposits and subordinate gravel and silt. It crops out around Mores, Mt. Ruju and Florinas, forming large- scale cross-stratified foresets up to 80 m thick, ranging in dip from 10° up to 20° and dipping SE-wards (Fig. 5A, B). Foresets of Facies B_1 have angles ranging from 12° to 22°, exhibit a *quasi*-tabular geometry or pinching out in both up- and down-dip directions, forming up to 2 m- thick beds (Fig. 6A, B). The sedimentary deposits belonging to this facies consist of 'pin-stripe' alternating 5–10 cm-thick sandstone beds (sub-fa- cies B_{1a}) intercalated with 0.3–0.5 m-thick siltstone beds (sub-facies B_{1b}) (Fig. 6C). Sandstone beds thin down-dip, whereas they thicken up-dip, passing into sub-horizontal beds through offlap breaks (Fig. 6B). Locally the fine-grained intervals show anomalous thicknesses up to 10 m, with loading and scouring structures (Fig. 6D). The sand- stone intervals (sub-facies B_{1a}) are made up of moderately- to poorly- sorted medium-to-very coarse sandstone, exhibiting sub-angular to rounded clasts (ca. 70% of quartz, 15–20% of alkali feldspars and very rare volcanics) and including sub-rounded pebbles (ca. 5–10%) inter- spersed in a kaolinitic matrix (Fig. 6E). All these elements are interspersed in ca. 10–15% of matrix made up of clay minerals. In the Mores and Florinas areas, strata show

erosional bases (Fig. 6F, G), either normal or reverse graded (Fig. 6F, G) or display bipartite grain-size zones, where coarse-grained, massive sandstone is abruptly overlain by fine-grained sandstone (Fig. 6G). The siltstone intervals (sub-facies B_{1b}) appear structureless or are faintly laminated (Fig. 6C). Facies B_1 lacks macrofossils and bioturbation, except for rare vertical traces observed in the sandstone strata.

5.4.2.

Quarry exposures in the Florinas area show large-scale foresets forming at least two vertically stacked clinoform units, each up to 30 m thick and separated by a major discontinuity. This latter is marked by top-lap stratal terminations of the underlying unit and down-lap terminations of the overlying one (Fig. 3, Log #3; Fig. 5B, C). Here, a 25 m-thick interval sandwiched between foresets includes plastically deformed bedding, with folds showing axes oriented down-dip to southeast (Fig. 3, Log #3; Fig. 5B, C). These features are associated with isolated scours and chute-and-fill structures at variable strati- graphic heights of the lower foreset unit (Fig. 3, Log #3; Fig. 6D).

5.4.3. Facies B_2: mixed, siliciclastic-bioclastic delta-platform deposits

Facies B_2 consists of mixed, siliciclastic and bioclastic deposits, inter- nally including up to three main orders of sub-horizontal cross stratifi- cation. 1st-order discontinuities are regular erosional surfaces bounding tabular sand bodies ranging in thickness from 5 to 22 m (Fig. 7A). Internally, they exhibit 2nd-order discontinuities forming unidirectional, NW-trending foresets (2nd-order cross bedding), with angular and tangential geometries (Fig. 7B, C). In turn, these foresets contain 3rd-order discontinuities, bounding minor foresets (3rd-order cross bedding), ranging in thickness from 0.5 m to 10 m and visible along strike-oriented exposures (Fig. 7D–F). Palaeocurrents indicate high angles with respect to the 2nd-order foresets, pointing towards W-SW in the thicker cross beds and towards N-NE in the thinner ones. Sediments of Facies B_2 exhibit two main scales of mixing: a 'compo- sitional mixing' (e.g., within the 3rd-order cross bedding) and a 'strata- mixing' (within the 2nd-order cross bedding) (cf., Chiarella et al., 2017). Facies B_2 includes two sub-facies: the siliciclastic-rich B_{2a} and the bioclastic-rich B_{2b}. Both sub-facies form elongate narrow sand bodies, up to 1 km long and 70 m wide, well exposed in the Ploaghe area (Fig. 2A). The siliciclastic-rich sub-facies B_{2a} consists of moderately- to poorly-sorted medium-to-very coarse sandstones with calcite cement, exhibiting a chaotic textural fabric and with a *b/s ratio* (cf., Chiarella and Longhitano, 2012) $\ll 1$ (20% of bioclasts vs. 80% of siliciclastic grains) (Fig. 7G). Mineralogical composition is similar to that observed in the underlying Facies B_1. The large amount of quartz and alkali feldspar detected in outcrop is visible also at thin-section scale. Samples collected in the Ploaghe area show grains partially cemented by second- ary (authigenic) calcite filling the inter-particle pores. Quartz often exhibits undulate extinction, whereas the clay minerals derives from chemical weathering of alkali feldspar. Among others, orthoclase has frequently perthitic intergrowths (Fig. 7H, I). Two groups of plagioclase occurs: the first group includes grains weathered in clay mineral and saussurite; the second group shows euhedral and unweathered grains (Fig. 7J, K). Abundant fossils are present, including shells of *Chlamys*, preserved entirely or in fragments, and echinoids, particularly *Amphiope hollandi*, *Clypeaster intermedius* and *Scutella sardica* (Martini et al., 1992). These deposits are in places highly bioturbated (BI = 3), show- ing sub-horizontal trace fossils of *Cruziana*, in particular belonging to *Repichnia*/*Paschnia* categories (Ekdale et al., 1984) (Fig. 7L).

The bioclastic-rich sub-facies B_{2b} shows a *b/s ratio* $\gg 1$ (80% of bioclasts vs. 20% of siliciclastic grains). It is intercalated with terrigenous sub-facies B_{2a} in the Ploaghe area, forming lenticular levels up to 5 m thick (Fig. 2B, C). Sub-facies B_{2b} has an erosional basal contact and is organised into vertically stacked, amalgamated, tabular to lenticular 3rd-order cross beds (average thickness of 20 cm) (Fig. 7D). Thin- sections (Fig. 7H, I, J, K) reveal

grainstone and packstone which, in places, become an algal-rich floatstone/rudstone, containing carbonate matrix and sparite. Echinoids, ostreids, rodoliths, pectinids, bryozoans and foraminifera, well preserved or in fragments, represent the macro- fossil content. Ichnotraces of *Skolithos* are sparsely present.

5.4.3.1. *Interpretation.* Facies association *B* represents deposits accumu- lated in different deltaic subaqueous environments, developed along discrete segments of the margins of this part of the Sardinian Seaway and generating large-scale topset-foreset architectures. The lack of bottomsets can be attributable to the absence of sections revealing the lowermost interval of the succession, rather than to a depositional motif (i.e., foresets with angular geometry).

Facies B_1 records sedimentation along a gravity-dominated, current- influenced delta-slope environment (Bhattacharya and Walker, 1992; Reading and Collinson, 1996; Bhattacharya, 2010), where sediments accumulated by gravity-driven density flows (Nemec, 1990). This type of setting was steep enough to trigger gravitational collapse of packages of foreset strata which, after detachment and consequent down-dip slumping, arrested their motion at the delta slope toe forming thick chaotic interval bearing soft-sediment deformation structures and intercalated between undeformed foresets (Fig. 8A, B). Mass-wasting processes are also suggested by deposits with internal muddled fabric filling spoon-shaped scours and chute structures visible in the lower- most foreset interval exposed in the Florinas quarry (Fig. 5B, C). In this setting, turbidity and debris flows represented background processes, as they have been broadly described in submerged deltaic slope environments (e.g., Postma, 1990; Longhitano, 2008). In the coarse- grained intervals (Facies B_{1a}), erosional bases of the single strata-sets and the normal grading textures support this interpretation. Orientation and imbrication of granules and pebbles are attributable to the effect of shear stress exerted along basal surfaces. High-density debris flows produce reverse grading: coarser clasts are pushed upwards by dispersive pressure and finer grains percolate downwards due to kinetic sieving (Nemec, 1990). The vertical grain-size segregation observed in some outcrops is interpreted as bipartite turbidity currents, composed of a basal high-density flow, which turned into turbulent flows during its downslope motion (Mutti et al., 1999, 2003). The sedimentary record of this process is represented by traction deposits of coarse material occurring in the lowermost bed interval, which is sharply capped, through a bypass surface, by finer-divisions deposited by the dilute tail of the turbidity current.

The poorly sorting of B_{1a} sandstone is attributed to secondary (authigenic) chemical weathering of alkali feldspars, producing a kaolin- itic matrix (Fig. 6E). The absence of fossils and low bioturbation index point towards a high rate of sandstone accumulation and stressful condi- tions for infaunal colonisation of organisms (MacEachern et al., 2005).

The fine-grained intervals (sub-facies B_{1b}) record settling of sedi- ment from suspensions or, when they exhibit anomalous thicknesses, stages of delta abandonment due to delta-lobe switching processes (e.g., Nemec, 1990; Postma, 1990).

The cross-stratified narrow/linear sand bodies of Facies B_2 are interpreted as longshore-migrating dunes forming dip-elongate bedform fields in a current-influenced delta-platform environment (Weise, 1980; Willis, 2005; Olariu et al., 2012; Longhitano and Steel, 2016; Rossi et al., 2017; Longhitano, 2018b). 1st-order surfaces of Facies B_2 display topset geometries overlying foresets of Facies B_1. In the Ploaghe section (Figs. 7B, C, 8A, C), 2nd-order cross beds of sub-facies B_{2a} represent siliciclastic large dunes, moving in a paleo-direction approximately perpendicular to the deltaic progradational axis, which seems to be typical of frontal sectors of deltas impinging current- dominated narrow receiving basins (Longhitano and Steel, 2016). 3rd-order cross

bedding reflects minor bedforms superimposed onto the larger ones during shorter time intervals. Since their directions of migration (W-SW and N-NE) reflect trajectories oriented at high angle with respect to the main net-gross sediment transport pathway (W- NW), these bedforms could reflect secondary residual currents, possibly triggered by waves.

The overall textural immaturity of sediments indicates that deposi- tion occurred very rapidly, after river-dominated flooding episodes. Currents affecting delta-platform areas reworked these deposits.

The co-existence of two diachronous generations of plagioclase, the first and older generation composed of weathered grains, the second and younger showing euhedral and unweathered grains (Fig. 7J, K), sug- gests that the 'Sabbie di Florinas' Fm deposition, in general, and dunes of sub-facies B_{2a}, in particular, resulted dominantly from a primary source (i.e., river deltas). However, a secondary source related to the erosion of exposed substrate blocks in subaqueous conditions and consequent recycling of the first sedimentary sequence during transgression is also invoked. It is not excluded, also, that the 'Sabbie di Florinas' were subject to further erosion and reworking after emplacement, as indi- cated by weathering of plagioclase, as well as by the occurrence of several orders of erosional discontinuities at various stratigraphic heights (Fig. 7D, E).

Marine trace fossils found in this facies are consistent with a shallow-marine high-energy setting (e.g., Scasso et al., 2012). *Cruziana* traces may be indicative of localised areas relatively protected from the main currents, e.g., troughs between major dunes or their toesets (MacEachern et al., 2012). The 3rd-order carbonate cross beds of sub- facies B_{2b}, which are intercalated within sub-facies B_{2a}, record sudden and episodic changes of sediment source, from siliciclastic to dominantly bioclastic. This 'strata mixing' (cf., Chiarella et al., 2017) is docu- mented in other ancient deltaic settings (Santisteban and Taberner, 1988) and attributed to episodes of delta-lobe switching, during which the main siliciclastic source is deflected laterally, favouring colo-nisation of the delta front. Alternatively, it may represent decreasing riverine run-off and more optimal conditions for the development of carbonate factories. Processes governing the accumulation of these bioclastic-rich intervals were still influenced by bed-shear stress exerted by along-shore currents, which affected the delta front environ- ment, as during deposition of siliciclastic dunes.

5.5. *Facies association C: current-dominated siliciclastic-to-carbonate sea- way deposits*

5.5.1. *Description*

Facies association *C* includes three facies, C_1, C_2, and C_3, which form the uppermost stratigraphic interval at Mores, Mt. Santo and Ploaghe (Fig. 3). The deposits lie on a basin-scale erosional surface (*tr1*, Figs. 3, 9A, B) and dominantly consist of bioclastic strata with sub- ordinate siliciclastic intervals, with a total thickness of 50–60 m.

5.5.2. *Facies C_1: tidal dune deposits*

Sub-facies C_1 crops out at Florinas and Ploaghe reaching a total thick- ness of 20 m. This facies includes two sub-facies: the terrigenous sub-facies C_{1a} and the mixed siliciclastic/bioclastic sub-facies C_{1b} (i.e., 'compositional mixing'; cf., Chiarella et al., 2017). Sub-facies C_{1a} consists of heterolithic coarse- to very coarse-grained sandstone and fine-grained sandstone, compositionally similar to underlying sub-facies B_{2a}, with quartz (dominantly) and alkali feldspars in a sparite or in a kaolinitic matrix (Fig. 9C). However, this facies exhibits a higher degree of textural maturity when compared with underlying strata, with well-rounded quartz clasts and good sorting. Fragments of shells and echinoids are sparsely present. Bioturbation structures occur in dis- crete horizons (BI = 1–3), forming predominantly horizontal and verti- cal dwelling burrows, as well as mobile

deposit-feeding traces (i.e., *Cruziana*, in particular repichnia and paschnia, *Rosselia* and (?) *Macaronichnus*) (Fig. 9C, D). At the top of the succession exposed in the Florinas quarry, sub-facies C_{1a} is made up of indistinctly cross- stratified sandstone with carbonate cement lying on an undulating erosional contact to the underlying delta-platform deposits of Facies B_1 (*tr1*, Figs. 3, 9B).

In the Ploaghe area, sub-facies C_{1a} erosionally overlies sub-facies B_{2a} and exhibits a maximum thickness of ca. 5 m (Fig. 9A). Sediments are organised into medium-scale cross-sets bounded by 1st-order disconti- nuity surfaces, including foresets with a general S-SW direction of accre- tion. Internally, 2nd-order discontinuities are highlighted by lamina pinch-out with no significant grain-size changes. Single strata locally exhibit foresets migrating in the opposite direction (N-NE) to the gen- eral palaeocurrent trend (Fig. 9D). Repeated thinning-to-thickening intervals of lamina bundles, associated with fining-to-coarsening lamina-sets, are frequent and intermittently interrupted by discontinu- ity (reactivation) surfaces (Fig. 9C).

The mixed sub-facies C_{1b} forms a 3 to 8 m-thick succession overlying sub-facies C_{1a}. The basal boundary is erosional and often characterised by up to 50 cm-deep and 90 cm-wide scours or gutter casts (Fig. 10A), associated with *Skolithos* ichnofacies (including *Skolithos* and *Ophiomorpha* traces) (Fig. 10B, C) and shell patches (Fig. 10D). A matrix- to clast-supported assemblage of coarse-grained particles (mainly quartz and feldspar) fills such gutter casts, including randomly dispersed disarticulated bivalve, echinoid and minor algal fragments (Fig. 10D, E). At the base, sub-facies C_{1b} exhibits locally cross-stratified strata sets with bi-directional foresets (Fig. 9D). Up- wards, cross bedding exhibits clast-supported coarse-grained particles and randomly dispersed bioclasts. Locally, discontinuity surfaces are highlighted by aligned 5–10 cm-thick and 10–15 cm-wide scours (gutter casts) filled exclusively by bivalve shells (Fig. 10F, G).

5.5.3. *Facies C_2: bioclastic ridges*

Facies C_2 erosionally overlies the underlying Facies C_1 in the Ploaghe area (Fig. 9A) and occurs intercalated with Facies B_1 (Mt. Santo; Figs. 2C, 3). The deposits are dominantly bioclastic and have elon- gated and narrow shape in plan view, both in marginal and axial sectors of the Logudoro Basin. It includes two sub-facies: C_{2a} and C_{2b}.

Sub-facies C_{2a} crops out only in the Mt. Lachesos section (north of Mores), where Facies C_2 exhibits elongate NNE-SSW-trending 2 km- long and 3 km-wide depositional geometries (Fig. 11A, B). Sub-facies C_{2a} lies at the base of the measured section and passes upwards to sub-facies C_{2b}, reaching a maximum thickness of 5 m (Figs. 3, 11C). Sub-facies C_{2a} is a mudstone and wackstone, with floating very coarse-grained bioclastic particles. It forms heterolithic plane-parallel stratification (from one to few dm thick), showing in places amalgam- ated beds and intensely bioturbated by, most probably, arthropods and worms (BI = 4) (Fig. 11D, E). Sub-facies C_{2b} forms up to 20 m- thick lenticular carbonate deposits dominantly formed by accumulation of shell fragments. In dip-oriented sections, the sub-facies presents m-scale low angle plane-parallel stratification. Internally, smaller-scale cross beds (15 to 50 cm-thick) show palaeocurrents with bimodal direc- tions but oriented at a high angle, when compared to the orientation of major (1st-order) accretion surfaces (Fig. 11A, B, F). Strike-oriented sec- tions are visible at Mt. Lachesos and Mt. Santo sections (axial sector of the Logudoro Basin), where clinoform geometries are observable (Figs. 11A, F, 12A, B). Bottomsets show low-angle cross-stratified cosets, some tens of centimetres thick (Fig. 12C). Strata are normally graded, with tabular, lenticular and sigmoidal shapes. Internally, single beds show indistinct foresets, dipping in the opposite direction of master bedding (Fig. 12D). Only scarce vertical ichno-traces are present. Thin-section observations reveal grainstone and floatstone with

alloch- thonous rhodolith nodules, echinoid plates, fragments of bryozoa, large benthic foraminifera (rotaliniids and textulariids) and planktonic foraminifera (Fig. 12E, F). The matrix consists of small bioclasts, calcite cement and clays (Fig. 12E, F).

In marginal sectors of the basin (i.e., Ploaghe), Facies C_2 shows up to 10 km-long and 2 km-wide NNW-SSE-trending elongate deposits, including at least three overlapping stratigraphic units (Fig. 13A, B). The dip direction of the internal cross-bedding in the sub-facies C_{2b}, doc- uments a southwest migration of such bodies through time (Fig. 13B). Measured palaeocurrents have directions rotating upwards from N160E to N210E (Figs. 3, 13B). In the Ploaghe section, the sub-facies C_{2b} is characterised by a plane-parallel nodular strataset, having an average thickness of 10 cm (Fig. 13C) and forming a succession up to 10 m thick. Thin-section observations reveal grainstone and floatstone rich in red algal nodules (Fig. 13D) and containing benthic foraminifera (rotaliniids and textulariids) in a carbonate matrix and sparite (Fig. 13E, F).

5.5.3.1. *Interpretation.* Facies association *C* is interpreted to represent a rapid marine transgression responsible for a tide-dominated setting, which succeeded deltaic sedimentation. The basal erosion surface (i.e., *tr1*), which can be followed for kilometres across the Logudoro Basin, represents a type of tidal ravinement promoted by energetic tidal currents in a seaway setting (cf., Longhitano and Steel, 2016).
This transgressive surface differs from the more 'classical' tidal ravinement detected in estuarine settings (e.g., Zaitlin et al., 1994), where erosion is exerted by the entrenchment of tidal channels onto underlying fluvial deposits in coastal areas as consequence of landward migration of the zone of maximum tidal energy (e.g., Swift, 1968; Allen and Posamentier, 1993).

The abundance of current-related architectures noted at various scales within the deposits of Facies Association *C* (from large-, to medium- to small-scale cross stratification; cf., Ashley, 1990) indicates a high-energy subaqueous scenery, possibly representing discrete parts of a wide marine seaway (e.g., Longhitano, 2013). This subaqueous conduit was presumably crossed by tidal currents, flowing axially and capable of reworking large volumes of sand mostly derived from erosion of underlying delta-front deposits and forming extensive bedform fields. Subaqueous winnowing is suggested by the textural maturity of the siliciclastic sediments and their compositional similarities with underlying deposits. Sub-facies C_{1a} and C_{1b} are interpreted as superimposed siliciclastic and bioclastic tidal dunes, respectively, generated by bi-directional tidal currents, as indicated by internal reactivation surfaces and reversal directions of foreset lateral accretion. Ebb-flood and neap-spring tidal cyclicities are indicated by internal lamina bundling of sub-facies C_{1a} (e.g., Allen and Homewood, 1984; Dalrymple, 2010; Longhitano et al., 2012a, 2012b). In these latter deposits, tidal structures lack distinct mud drapes as the system was mud-poor and the sand is overall coarse grained, which is typical of high-energy tidal strait-fill cross strata (e.g., Longhitano and Nemec, 2005). In sub-facies C_{1a}, *Cruziana* ichnofacies reflects localised areas protected from the main currents, whereas the degree of bioturbation (BI = 1–3) indicates variable rates of dune migration. Sub-facies C_{1b} is thus interpreted as the record of a current-dominated seaway environment, hosting dunes deflected by longshore currents. Cross stratification and opposite directions of foresets, as well as the presence of gutter casts within the facies, suggest periodic changes in strength and direction of flows, documenting a tidal influence (e.g., Longhitano et al., 2012a).

The erosional boundary between sub-facies C_{1b} and the underlying deposits of sub-facies C_{1a} (i.e., *tr2*) is represented by a sharp surface that can be attributed to localised current acceleration and consequent scouring (e.g., lineations; see Stow et al., 2009). Scours similar to those described within this association (i.e., gutter casts) are typical of sub- aqueous zones exposed to the action of strong bottom currents, up to 2 m s^{-1} (e.g., Mitchell

et al., 2013; Hernández-Molina et al., 2016).

Current acceleration may have been due to: (i) lateral flow constrictions (i.e., sediment build-ups) of the main sedimentary routes; (ii) episodes of relative sea-level lowering and consequent reduction in cross- sectional area of subaqueous basinal sectors; and/or (iii) changes in the dynamics of oceanographic processes, enhanced by episodic storms or other episodic events.

The *tr2* surface also documents a lithological change (from siliciclastic to mixed and calcareous deposits) within the overall transgressive trend. In the Logudoro Basin carbonate deposits of sub- facies C_{1b} and Facies C_2 were presumably sourced by autochthonous, short-lived carbonate factories, as also documented in other settings of the Neogene-to-Quaternary record of Sardinia (e.g., Andreucci et al., 2017) and other central Mediterranean areas (e.g., Catalano et al., 1998; Pomar and Tropeano, 2001; Massari and Chiocci, 2006).

Facies C_2 is interpreted as tidal shelf ridges (e.g., Snedden and Dalrymple, 1999; Berné et al., 2002; Wang et al., 2012; Messina et al., 2014) developed in a current dominated seaway. This facies overlies deltaic deposits through a transgressive erosive surface (*tr1*) (Belderson et al., 1982; Liu et al., 1998; Berné et al., 2002; Wang et al., 2012).

Heterolithic deposits of sub-facies C_{2a} mark the transition towards a marginal portion of the ridge (offshore and offshore-transition deposits; Leva-López et al., 2016). The association of heterolithic successions and the abundant trace fossils of arthropods and worms are typical of shelf deposits, where low-energy conditions and abundant organic particles, settled from suspension onto the sea floor, occur (Desjardins et al., 2012).

Sub-facies C_{2b} probably records ridge-nucleus deposits, composed predominantly of large-scale cross-bedded carbonates. The presence of scarce vertical traces in such cross-stratified beds clearly indicates closed to short-term colonisation windows linked with the rapid upward growth and down-current migration of the ridge (Desjardins et al., 2012). The smaller-scale cross-stratified beds dipping mainly at high oblique angle relative to the orientation of the larger-scale accretion surfaces may be explained as actively accreting bar surfaces with compound dunes (Leva-López et al., 2016; see inset in Fig. 12B). This is a characteristic feature of tidal-shelf ridges (e.g., Dalrymple, 2012; Rossi and Steel, 2016; Chiarella et al., 2020).

6. Discussion

6.1. *From an isolated endorheic basin to a marine seaway*

The Logudoro basin-fill succession includes three main sedimentary sequences, the first two of which are better preserved and separated by a late Langhian and/or early Serravallian regional angular unconformity. (Martini et al., 1992; Funedda et al., 2000, 2003). The first sequence (? Middle Burdigalian-early Langhian) includes terrestrial to marginal- marine conglomerates and sandstones, recording an endorheic setting (Fig. 14A), which evolved later to a shelf setting represented by a thick sequence of marlstones and siltstones (Fig. 14B), reflecting a generalised phase of basin deepening and marine inundation. At this time, no current or tidal signatures are detectable in these sediments, possibly due to no favourable conditions for water mass convergence or amplification, which can be typical of sheltered coastal embayments (e.g., Sztanó and de Boer, 1995; Longhitano, 2011). The second sequence developed after the middle Langhian dramatic sea-level drop (Mazzei and Oggiano, 1990; Martini et al., 1992) (Fig. 14C). A new stage of continental sedimentation in the Logudoro Basin led to the deposition of braid plains or large alluvial fan systems, sourced from the western and eastern margins, including rivers and inter- channel areas (Facies association *A*; Fig. 14D). These terrestrial

deposits are today observable in isolated sectors located in the axial part of the basin, probably because they record the initial stage of an incised valley- fill, being thus preserved thanks to their less elevated position between interfluve areas (Fig. 14D). The overall sandy grain size of the fluvial deposits and the absence of estuarine-type facies should reflect overfilled incised-valley fills accumulated during an early transgressive phase (Simms et al., 2006). Fluvial channels evolve from braided to ephemeral streams of lower energetic conditions, and rest laterally adjacent to inter-channel overflow deposits. The vertical transition from braided to ephemeral streams could reflect the exceedance of the rate of accommodation over the rate of sediment supply (A/S N 1), due to acceleration of relative sea-level rise (Cattaneo and Steel, 2003). This trend in accommodation is attributable to activity of the marginal fault systems on the SW side of the Logudoro Basin (Funedda et al., 2003). After this first stage of late lowstand or early transgression, the basin turned into a 10 km-wide and 20 km-long ma- rine area, representing the northern segment of the larger Sardinian Seaway (cf., Longhitano et al., 2017) (Fig. 14E).

6.2. *The opening of the Logudoro gateway: the first record of a current- dominated setting*

The Serravallian stratigraphic interval of the Logudoro Basin records an important oceanographic phase of basin interconnection. As relative sea level continued to rise, submerged marine delta facies (i.e., slope and platform deltaic deposits of Facies association *B* back-stepped onto the underlying terrestrial deposits) (Fig. 14E). This is particularly evident from the southwestern sector of the Logudoro Basin (e.g., at Mt. Santo; Fig. 2C), where the sedimentary deposits included in such intervals are mud-poor. This feature is common in deltaic successions prograding into current-dominated straits (Longhitano and Steel, 2016), due to the minor or no deposition (or preservation) of fall-out fines because of the high-energy setting of the receiving basin (e.g., Ayranci and Dashtgard, 2016; Rossi et al., 2017). Delta slopes in the Logudoro Basin exhibit pronounced gravity-dominated foresets, passing upwards into current-dominated delta platforms, made up of coarse-grained deposits. Delta platform facies suggest continuous sediment remobilisation by traction currents flowing parallel to the paleo-margins, where they may have had less influence on the deeper slope-deltaic facies. Siliciclastic sediments feeding delta slopes originated from erosion of marginal areas, as documented by the petro- graphic dataset. The same source also supplied overlying marine sediments of the delta platforms, although a minor percentage of clastic particles was also produced after erosion of underlying older units. This may have occurred after subaqueous sweeping, possibly exerted by strong currents, as testified by the presence of diachronous generations of plagioclase. Deposits of Facies Association *B* thus indicate the first early interconnection among the southern and the northern reaches of the Logudoro Basin with adjacent basins and the onset of a current-dominated oceanographic setting typical of a marine seaway (Dalrymple, 2010; Longhitano et al., 2012a; Longhitano, 2013) (Fig. 14E). This stage of oceanographic opening followed a prolonged phase during which this part of Sardinia was formed by isolated endorheic basins (Fig. 14A–D). Basal deltas are typical of settings where tectonics is actively producing accommodation space (Gawthorpe and Colella, 1990). This setting justifies the considerable thickness of the documented foreset stacking patterns and the presence of at least two or more generations of deltas separated by internal discontinuities (e.g., Colella, 1988). In addition, the development of an extensive subaqueous dune field in the delta platform setting of the Ploaghe area (Fig. 7B–F), suggests a relatively more gently sloping margin (e.g., Longhitano and Steel, 2016), when compared with Florinas and Mores margins. The present-day dip of the succession near Ploaghe is thus

attributed to syn-depositional tectonic tilting due to the presence of a marginal fault system (Funedda et al., 1999; Carmignani et al., 2012) rather than a primary depositional gradient (Martini et al., 1992).

During this marine stage, the Logudoro Basin would have been characterised by a complex topography, represented by several intra- basinal highs separating local bathymetric lows (Martini et al., 1992) (Fig. 14E). This assumption is supported by the high variability of thick- ness of the Sabbie di Florinas Fm (see cross-sections in Fig. 2C), which suggests as an inherited basin bathymetry may have also lead to a variable preservation potential of the transgressive deposits. During this first stage of seaway opening, no tidal influence occurred in the basin, probably because of the absence of oceanographic restrictions generating local tidal amplification or the sub-basins not wide enough to receive the effect of astronomical tides (e.g., Reynaud and Dalrymple, 2012).

The transition to seaway conditions was possibly driven by tectonic control exerted by a roughly E-W-oriented transfer zone located at the boundary separating the Logudoro from the Porto Torres basins (Funedda et al., 2000, 2003) (see Fig. 1B). This structural element is thought to represent one of the strike-slip fault systems that affected northern Sardinia from the late Oligocene-Aquitanian with a general left-lateral displacement (Carmignani et al., 1995; Oggiano et al., 1995; Pasci et al., 1998; Funedda et al., 2000). Although many authors do not consider this transfer zone as particularly active during the Serravallian-Tortonian time span (e.g., Faccenna et al., 2002; Dieni et al., 2008), it may have played some role in shaping the gateway and keeping connections between the Logudoro with the Porto Torres basin (Fig. 14E–F). Thanks to this structural controlled linkage, tidal amplification then affected sedimentation recorded in the studied stratigraphic interval.

6.3. *The onset of the tidal circulation in the Logudoro gateway*

As relative sea level continued to rise, the Logudoro gateway wid- ened (Fig. 14F), possibly presenting an oceanographic setting or bathy- metric features more prone to receive tidal influence compared with the previous stage (e.g., Anastas et al., 2006). Indeed, a clear tidal signature is recognizable within the marine deposits recording such relevant evolutionary phase of the basin (Fig. 9B–D). Herringbone tidal cross bedding, tidal bundles and lamina-scale segregation, associated with higher rates of textural and compositional maturity of the deposits, are all physical elements indicative of dominant tidal processes (e.g., Longhitano et al., 2012a). The onset of tidal circulation in the Logudoro gateway was possibly promoted by wider seas (Longhitano et al., 2012a). At this evolutionary stage (Fig. 14F), tidal currents were capable of reworking large volumes of sand along the margins, mostly derived from subaqueous erosion of the underlying delta-front deposits, forming subaqueous dunes. In the axial sectors of the seaway, extensive bedform fields developed, possibly reflecting depositional areas of the seaway separating zones of bypass and erosion (e.g., Longhitano, 2013). Water-depth estimations in the Logudoro Basin during marine flooding were empirically evaluated by using average cross strata-set thickness as an approximation of primary dune height (Best and Fielding, 2019). Median relation for predicting flow depth was derived from field data presented by Bradley and Venditti (2017). These authors suggest an approximation of the flow depth (Y) as ca. 6.7 of the dune height (H). Based on this theoretical approach, cross beds observed on delta platforms, recording siliciclastic and bioclastic-rich dunes b5 m thick (Facies B2) indicate a depth interval ranging from 28 to 55 m. Dunes and ridges of the overlying interval (Facies C1 and C2) with variable thickness ranging from 0.5 to 22 m, suggest a depth increasing up to ca. 150 m, as a final effect of the transgression.

Tidal currents parallel to basin margins promoted bioclastic ridges (Fig. 14F), reflecting a temporary decrease of siliciclastic input or zones of the seaway sufficiently far from siliciclastic source points (e.g., Santisteban and Taberner, 1988). In the Ploaghe area, the direction of migration of such ridges progressively switches towards the SW (sub facies C_{2b}), recording a rotatory pattern probably induced by oceano- graphic adjustment of tidal circulation of the seaway (Fig. 13A).

Internally, cross-stratified strata sets and herringbones are the main sedimentary evidence of deposition related to currents rhythmically changing in strength and direction (Kvale et al., 1989; Dalrymple et al., 1991; Klein, 1998; Coughenour et al., 2009). The micro-facies and micro-fossil assemblages observed in the bioclastic tidal dunes (sub facies C_{1b}; Fig. 12E, F) and in the bioclastic ridges (sub facies C_{2b}; Fig. 13D, E, F) corroborate the reconstruction of a high energy depositional setting. These and other evidences, including the various scales of cross bedding, the orderliness of internal discontinuities and the occurrence of shell-filled subaqueous scours (i.e., sub-facies C_{1b}, etc.) all support a dominance of marine currents over other basinal processes (e.g., oceanographic and internal waves, fluvial floods or den- sity currents).

Axial bioclastic ridges (e.g., at Mt. Santo and Mt. Lachesos) suggest the development of autochthonous heterozoan carbonate factories promoted by calcareous organisms adapted to energetic conditions and to a contemporaneous paucity of siliciclastic input. Switch-on of bioclastic-dominated sedimentation in the Logudoro Basin during this last stage of marine transgression could be related to more favourable climatic conditions: i.e., temperate marine waters, enrichment in nutri- ents, solar light penetration and well oxygenated clearer marine waters, salinity, Ca^{2+} and CO_2 concentrations, Mg/Ca ratio, alkalinity, etc. (see Pomar et al., 2004). Such influencing climatic factors are thought to be common during episodes of relative sea-level change (e.g., Pomar and Ward, 1999). An alternative explanation may invoke general conditions of terrigenous sediment starvation, common to basins that undergo rapid transgression (Cattaneo and Steel, 2003; Longhitano, 2018b). The episodes of carbonate deposition are also associated with passive enrichment of volcanogenic and/or authigenic sedimentary particles in the sediments (e.g., Baum and Vail, 1988).

7. Towards the reconstruction of the Miocene Sardinian Seaway

Based on recent attempts to model the sedimentary dynamics of tidal straits and seaways (e.g., Anastas et al., 2006; Reynaud and Dalrymple, 2012; Longhitano, 2011, 2013; Longhitano and Chiarella, 2020), the present case study seems to reflect similarities, as well as some differences, from the proposed prototypes.

The depositional model inferred for tectonically controlled, narrow tidal straits (Longhitano, 2013) points out the existence of four depositional zones, laterally adjacent from the narrowest strait centre towards its terminations, with a bedload parting area dividing symmetrically such zones: i.e., with two opposite major depositional areas separated by a central by-pass zone, or with one major depositional area (see discussion in Longhitano, 2013). The signature of these zones is re- corded in four diagnostic facies associations, indicated by a number of comparisons between different ancient tidal strait-fill successions (e.g., Longhitano, 2011; Longhitano et al., 2012b; Longhitano, 2013; Longhitano et al., 2014; Rossi et al., 2017; Longhitano, 2018b). These associations document distinctive facies stacking patterns with individ- ual sedimentary features, indicative of specific depositional strait environments subject to varying tidal influence.

In the present case, the observed facies spatial distribution points to a tidal strait including a central by-pass and erosional zone, separating two depositional areas but both dominated by one stronger tidal phase. This apparent exception to a symmetrically-distributed tidal strait model including a 'bedload-parting zone' (cf.,

Harris et al., 1995) has been recently documented in the modern Messina Strait, separating Sicily from the Italian peninsula in the central Mediterranean (Longhitano, 2018a). Here, a tidal phase opposition between the two interlinked basins (i.e., the Tyrrhenian Sea to the north and the Ionian Sea to the south) generates collinear tidal currents, of up to 3 m s^{-1}. However, due to water-mass stratification driven by a marked difference in salinity and density, the north-directed tidal phase dominates over the south-directed phase, although they reach similar peak velocities across the strait centre (Brandt et al., 1999). The direct reflection of such density-driven tidal asymmetry on the strait bottom is the occur- rence of large bedforms migrating towards the dominant current phase (i.e., northwards) (Longhitano, 2018a).

In the Logudoro Basin, reconstruction of the principal direction of lateral accretion of the various elongated bodies (Facies C_2) indicates the main sediment transport routes throughout the basin. In particular, the internal architectures of shelf ridges (Facies C_2, Fig. 14F) suggest the occurrence of two reversal directions of migration oriented roughly parallel to the basin paleo-margins (Fig. 15). Such net-gross sediment transport patterns could be referred to the presence of separated flood (north-directed) and ebb (south-directed) tidal components (e.g., Li and O'Donnell, 1997; Dalrymple and Choi, 2007).

Results from the present study suggest the development of a large marine seaway with a micro-tidal regime (tidal range b 2 m; Flemming, 2005) in this part of the Mediterranean during the Miocene (Longhitano et al., 2017). Its evolution is related to episodes of marine connection in different parts of the area corresponding with the Sardin- ian Graben System and promoting the accumulation of sedimentary sequences diagnostically characterised by large-scale cross stratification in either siliciclastic and carbonate deposits (Fig. 16).

8. Conclusions

The present study suggests a new environmental interpretation of the Serravallian sand-rich stratigraphic interval deposited in the Logudoro Basin, during a major phase of tectonically-driven transgression. Our results, based on detailed field study of a number of stratigraphic windows, detect different stages of basin evolution, starting from endorheic continental sedimentation, towards a stage of initial marine inundation and culminating in a phase of basin widening and oceanographic connection with other adjacent basins. The identification of this latter stage contributes in the reconstruction of the Miocene Sardinian Seaway, suggests new interpretative scenarios for the palaeogeographic framework of this part of the western Mediterranean, and adds constraints for the analysis of long-term sedimentary processes in tidal straits and seaways.

In particular, these are main conclusions of the present work:

1. The 'Sabbie di Florinas' Fm records a vertical deepening-upward facies trend, indicating a Serravallian phase of marine transgression. Three sedimentary phases in the Logudoro Basin infilling, with differ- ent dominant sedimentary process, have been distinguished: (i) Late lowstand-early transgressive terrestrial deposits (including rivers and inter-channel areas in a fluvial braid plain) aggraded over pre- existing topographic lows. (ii) During the ensuing transgression, marginal-marine sediments sourced from eroded uplifted adjacent areas and belonging to river deltas back-stepped onto the basin margins. Delta-slope facies show conventional gravity-dominated foreset deposits. Overlying delta-platform facies exhibit cross- bedded coarse-grained deposits indicating the dominance of marine, alongshore currents over waves, river outflow and tides. Basinwards, current-dominated and gravity-influenced deltaic sequences correspond with cross-bedded thick sandstone successions, representing extensive bedform fields and interpreted as the sedimentary response to more vigorous currents affecting the axial zones of the basin. Textural and mineralogical properties documented in

these basinal facies indicate a clastic contribution from subaqueous erosion of underlying units. (iii) Late transgressive-to-highstand tidal mixed, well-sorted siliciclastic/bioclastic cross beds with good textural features and carbonate, algae-rich clinoforms suggest continuous subaqueous winnowing and deposition in a tide-dominated seaway setting.

2. From a series of isolated endorheic small basins, the Logudoro Basin
evolved into a large embayment and then formed a ca. 10 km-wide seaway, after oceanographic connection with northern and southern marine areas. This stage of marine interlinking, recorded in the *tr1* basin-scale discontinuity, marks a precise stage in the northern Sardinian Seaway, a current-dominated marine passageway episodically active during the Miocene
3. No significant tidal influence occurred during the first marine stage of basin inundation, probably because the absence of suitable conditions (e.g., critical size of the basinal cross-sectional area, ab- sence of amphidromic points, attenuation of the tidal power due to water flow friction and inhibition of a tidal cyclicity, etc.). Tidal hydrodynamics prevailed during the stage of widening of the Logudoro Basin, when the seaway experienced a more mature oceanographic setting. A clear tidal signature observed in bioclastic ridges is the sedimentary record of this stage, which reflects a change in the oceanographic setting.
4. The spatial distribution of deposits accumulated during late transgression points to the occurrence of a tidal strait, generated by structural mechanisms triggered with a major transfer zone linking the Logudoro and the adjacent Porto Torre Basin during the late Serravallian-Tortonian. The strait included a central by-pass and erosional zone, separating two depositional areas dominated by a stronger tidal phase (i.e., 'bedload-parting zone'). Based on the internal architectures of shelf ridges, the net-gross sediment transport pattern is oriented parallel to the paleo-margins, suggesting the presence of separated flood and ebb tidal currents possibly governed by Coriolis forcing.
5. The studied sedimentary succession exhibits large-scale cross stratification in siliciclastic or carbonate deposits like many others exposed along the Sardinian Graben System, supporting the existence of a north-south-elongated current-dominated seaway (i.e., the Sardinian Seaway), generated by extensional tectonics and experiencing a tidal circulation during Miocene episodic marine connections.

References

Allen, J.R.L., 1965. A review of the origin and characteristics of recent alluvial sediments. Sedimentology 5, 89–191.

Allen, P.A., Homewood, P., 1984. Evolution and mechanics of a Miocene tidal sandwave. Sedimentology 31, 63–81.

Allen, P.A., Posamentier, H.W., 1993. Sequence stratigraphy and facies model of an incised valley fill: the Gironde Estuary, France. Journal of Sedimentary Research 63, 378–391.

Anastas, A.S., Dalrymple, R.W., James, N.P., Nelson, C.S., 1997. Cross-stratified calcarenites from New Zealand: subaqueous dunes in a cool-water, Oligo–Miocene seaway. Sedimentology 44, 869–891.

Anastas, A.S., Dalrymple, R.W., James, N.P., Nelson, C.S., 2006. Lithofacies and dynamics of a cool-water carbonate seaway: mid-Tertiary, Te Kuiti Group, New Zealand. In: Pedley, H.M., Carannante, G. (Eds.), Cool-Water Carbonates: Depositional Systems and Paleoenvironmental Controls. 255. Geological Society of London, Special Publica- tion, pp. 245–268.

Andreucci, S., Pistis, M., Funedda, A., Loi, A., 2017. Semi-isolated, flat-topped carbonate platform (Oligo-Miocene, Sardinia, Italy): sedimentary architecture and processes. Sedimentary Geology 361, 64–81.

Archer, S.G., Steel, R., Mellere, D., Cullen, B., Blackwood, S., 2019. Response of Middle Juras- sic shallow marine environments to syn-depositional block tilting: Isles of Skye and Raasay, NW Scotland. Scottish Journal of Geology 55, 35–68.

Ashley, G.M., 1990. Classification of large-scale subaqueous bedforms; a new look at an old problem. Journal of Sedimentary Petrology 60, 160–172.

Assorgia, A., Barca, S., Casula, G., Spano, C., 1988. Le successioni sedimentarie e vulcaniche del Miocene nei dintorni di Giave e Cossoine (Logudoro, Sardegna NW). Bollettino della Società Sarda di Scienze Naturali 26, 75–107.

Ayranci, K., Dashtgard, S.E., 2016. Asymmetrical deltas below wave base: insights from the Fraser River Delta, Canada. Sedimentology 63, 761–779.

Barca, S., Ulzega, A., Melis, E., Orru, P., 2005. Foglio 557 "Cagliari". Carta geologica d'Italia in scala 1:50.000. ISPRA, Servizio Geologico d'Italia, Roma.

Barrier, E., Vrielynck, B., 2008. Paleotectonic Maps of the Middle-East. Atlas of the MEBE Program, 14 Maps to the 1:18 500 000 Scale. Pub. CCGM/CGMW, Paris.

Baum, G.R., Vail, P.R., 1988. Sequence stratigraphic concepts applied to Paleogene out- crops, Gulf and Atlantic Basins. In: Wilgus, C.K., Hastings, B.S., Kendall, C.G.St.C., Posamentier, H.W., Ross, C.A., Van Wagoner, J.C. (Eds.), Sea-Level Changes - An Inte- grated Approach. 42. SEPM Special Publication, pp. 309–327.

Belderson, R.H., Stride, R.H., 1966. Tidal current fashioning of a basal bed. Marine Geology 4, 237–257.

Belderson, R.H., Johnson, M.A., Kenyon, N.H., 1982. Bedforms. In: Stride, A.H. (Ed.), Off- shore Tidal Sands, Process and Deposits. Chapman and Hall, London, pp. 27–57.

Berné, S., Lericolais, G., Marsset, T., Bourillet, J.-F., Debatist, M., 1998. Erosional offshore sand ridges and lowstand shorefaces: examples from tide- and wave-dominated en- vironments of France. Journal of Sedimentary Research 68, 540–555.

Berné, S., Vagner, P., Guichard, F., Lericolais, G., Liu, Z., Trentesaux, A., Yin, P., Yi, H.I., 2002. Pleistocene forced regressions and tidal sand ridges in the East China Sea. Marine Ge- ology 188, 293–315.

Best, J., Fielding, C.R., 2019. Describing fluvial systems: linking processes to deposits and stratigraphy. In: Corbett, P.W.M., Owen, A., Hartley, A.J., Pla-Pueyo, S., Barreto, D., Hackney, C., Kape, S.J. (Eds.), River to Reservoir: Geoscience to Engineering. 488. Geo- logical Society, London, Special Publications, pp. 152–166.

Bhattacharya, J.P., 2010. Deltas. In: Dalrymple, R.G., James, N.P. (Eds.), Facies Models 4. 6. Geological Association of Canada, pp. 233–264.

Bhattacharya, J.P., Walker, R.G., 1992. Deltas. In: Walker, R.G., James, N.P. (Eds.), Facies Models: Response to Sea Level Change. Geological Association of Canada, pp. 157–177.

Bosworth, W., 1985. Geometry of propagating continental rifts. Nature 316, 625–627. Bradley, R.W., Venditti, J.G., 2017. Reevaluating dune scaling relations. Earth-Science Reviews 165, 356–376.

Braga, J.C., Martín, J.M., Aguirre, J., Baird, C.D., Grunnaleite, I., Jensen, B.N., Puga-Bernabéu, A., Sælen, G., Talbot, M.R., 2010. Middle-Miocene (Serravallian) temperate carbonates in a seaway connecting the Atlantic Ocean and the Mediterranean Sea (North Betic Strait, S Spain). Sedimentary Geology 225, 19–33.

Brandt, P., Rubino, A., Quadfasel, D., Alpers, W., 1999. Evidence for the influence of Atlantic-Ionian stream fluctuations on the tidally induced internal dynamics in the Strait of Messina. Journal of Physical Oceanography 29, 71–80.

Bridge, J.S., 1993. Description and interpretation of fluvial deposits: critical perspective. Sedimentology 40, 801–810.

Bridge, J.S., 2003. Rivers and Floodplains. Blackwell, Oxford, U.K., p. 491. Bridge, J.S., 2006. Fluvial facies models: recent developments. In: Posamentier, H., Walker, R.G. (Eds.), Facies Models Revisited. 84. SEPM Special Publication, pp. 85–170.

Cant, D.J., 1992. Subsurface facies analysis. In: Walker, R.G., James, N.P. (Eds.), Facies Models, Response to Sea Level Changes. Geological Association of Canada, pp. 27–45.

Capella, W., Hernández-Molina, F.J., Flecker, R., Hilgen, F.J., Hssain, M., Kouwenhoven, T.J., van Oorschot, M., Sierro, F.J., Stow, D.A.V., Trabucho-Alexandre, J., Tulbure, M.A., de Weger, W., Yousfi, M.Z., Krijgsman, W., 2017. Sandy contourite drift in the late Mio- cene Rifian Corridor (Morocco): reconstruction of depositional environments in a foreland-basin seaway. Sedimentary Geology 355, 31–57.

Carmignani, L., Barca, S., Disperati, L., Fantozzi, P., Funedda, A., Oggiano, G., 1994. Tertiary compression and extension in the Sardinian basement. Bollettino di Geofisica Teorica ed Applicata 36, 45–62.

Carmignani, L., Decandia, F.A., Disperati, L., Fantozzi, P.L., Lazzarotto, A., Liotta, D., Oggiano, G., 1995. Relationship between the Tertiary structural evolution of the Sardinian Corsica-Provençal Domain and the Northern Apennines. Terra Nova 7, 128–137.

Carmignani, L., Oggiano, G., Funedda, A., Conti, P., Pasci, S., Barca, S., 2012. Carta Geologica della Sardegna. Scala 1:250.000. LAC, Firenze.

Carminati, E., Doglioni, C., 2005. Mediterranean geodynamics. In: Selley, C., Cocks, L.R.M., Plimer, I.R. (Eds.), Encyclopedia of Geology. Elsevier, pp. 135–146.

Carminati, E., Lustrino, M., Cuffaro, M., Doglioni, C., 2010. Tectonics, magmatism and geodynamics of Italy: what we know and what we imagine. In: Beltrando, M., Peccerillo, A., Mattei, M., Conticelli, S., Doglioni, C. (Eds.), The Geology of Italy, Elec- tronic editionJournal of the Virtual Explorer, p. 36 https://doi.org/10.3809/ jvirtex.2010.00215 ISSN 1441-8142.

Casula, G., Cherchi, A., Montadert, L., Murru, M., Sarria, E., 2001. The Cenozoic graben sys- tem of Sardinia (Italy): geodynamic evolution from new seismic and field data. Ma- rine and Petroleum Geology 18, 863–888.

Catalano, R., Di Stefano, E., Sulli, A., Vitale, F.P., Infuso, S., Vail, P.R., 1998. Sequences and systems tracts calibrated by high-resolution bio-chronostratigraphy: the central Mediterranean Plio-Pleistocene record. In: de Graciansky, P.C., Hardenbol, J., Jaquin, T., Vail, P.R. (Eds.), Mesozoic and Cenozoic Sequence Stratigraphy of European Basins. 60. SEPM Special Publication, pp. 155–177.

Cattaneo, A., Steel, R.J., 2003. Transgressive deposits: a review of their variability. Earth- Science Reviews 62, 187–228.

Cattaneo, A., Miramontes, E., Samalens, K., Garreau, P., Caillaud, M., Marsset, B., Corradi, N., Migeon, S., 2017. Contourite identification along Italian margins: the case of the Portofino drift (Ligurian Sea). In: Longhitano, S.G., Steel, R.J., Pomar, L. (Eds.), Sedimentology in Italy: New Advances and Insights. Marine and Petroleum Geology 87, pp. 137–147.

Cherchi, A., Montadert, L., 1982a. Il sistema di rifting Oligo-Miocenico del Mediterraneo Occidentale e sue conseguenze paleogeografiche sul Terziario sardo. Memorie della Società Geologica Italiana 24, 387–400.

Cherchi, A., Montadert, L., 1982b. Oligo-Miocene rift of Sardinia and the early history of the Western Mediterranean Basin. Nature 298, 736–739.

Cherchi, A., Mancin, N., Montadert, L., Murru, M., Putzu, M.T., Schiavinotto, F., Verrubbi, V., 2008. The stratigraphic response to the Oligo-Miocene extension in the western Mediterranean from observation on the Sardinia graben system (Italy). Bulletin de la Société Géologique de France 179, 267–287.

Chiarella, D., Longhitano, S.G., 2012. Distinguishing depositional environments in shal- low-water mixed bio-siliciclastic deposits on the base of the degree of heterolithic segregation (Gelasian, Southern Italy). J. Sediment. Res. 82, 962–990.
Chiarella, D., Longhitano, S.G., Tropeano, M., 2017. Types of mixing and heterogeneities in siliciclastic-carbonate sediments. Mar. Pet. Geol. 88, 617–627.
Chiarella, D., Longhitano, S.G., Mosdell, W., Telesca, D., 2020. Sedimentology and facies analysis of ancient sand ridges: Jurassic Rogn Formation, Trøndelag Platform, offshore Norway. Mar. Pet. Geol. 112. https://doi.org/10.1016/j.marpetgeo.2019.104082.
Colella, A., 1988. Pliocene-Holocene fan deltas and braid deltas in the Crati Basin, southern Italy: a consequence of varying tectonic conditions. In: Nemec, W., Steel, R.J., (Eds.), Fan Deltas. Blackie & Son Ltd. London, pp. 50–74.
Collinson, J.D., 1996. Alluvial sediments. In: Reading, H.G. (Ed.), Sedimentary Environ- ments and Facies, Third edition Elsevier, New York, pp. 37–82.
Collinson, J.D., Mountney, N., Thompson, D., 2006. Sedimentary Structures. 3rd Revised edition. Dunedin Academic Press Ltd., London (304 p.).
Coughenour, C.L., Archer, A.W., Lacovara, K.J., 2009. Tides, tidalites, and secular changes in the Earth–Moon system. Earth Sci. Rev. 97, 59–79.
Dalrymple, R.W., 2010. Tidal depositional systems. In: James, N.P., Dalrymple, R.W. (Eds.), Facies Models 4. Geological Association of Canada, St. John's, pp. 201–231.
Dalrymple, R.W., 2012. Tidal depositional systems. In: James, N.P., Dalrymple, R.W. (Eds.), Facies Model 4. Geological Association of Canada, St. John's, Canada, pp. 201–231.
Dalrymple, R.W., 2019. Morphology, processes and facies of modern straits: variability and complexity dominate. Proceedings of the 34th Meeting of the IAS, 10–13 Sep- tember 2019, Rome, p. 637.
Dalrymple, R.W., Choi, K., 2007. Morphologic and facies trends through the fluvial– marine transition in tide-dominated depositional systems: a schematic frame- work for environmental and sequence-stratigraphic interpretation. Earth Sci. Rev. 81, 135–174.
Dalrymple, R.W., Makino, Y., Zaitlin, B.A., 1991. Temporal and spatial patterns of rhythmite deposition on mudflats in the macrotidal Cobequid Bay–Salmon River es- tuary, Bay of Fundy, Canada. In: Smith, D.G., Zaitlin, B.A., Reinson, G.E., Rahmani, R.A. (Eds.), Modern and Ancient Clastic Tidal Deposits. Canadian Society of Petroleum Ge- ologists. 16, pp. 137–160.
Daniell, J.J., 2015. Bedform facies in western Torres Strait and the influence of hydrody- namics, coastal geometry, and sediment supply on their distribution. Geomorphology 235, 118–129.
Davis, R.A., Balson, P.S., 1992. Stratigraphy of a North Sea tidal sand ridge. J. Sediment. Pet- rol. 62, 116–121.
Dercourt, J., Gaetani, M., Vrielynck, B., Barrier, E., Biju-Duval, B., Brunet, M.-F., Cadet, J.-P., Crasquin, S., Sandulescu, M., 2000. Peri-Tethys Palaeogeographic Atlas, 1 Volume and 24 Maps at 1:10 000 000 Scale. Pub. CCGM/CGMW, Paris.
Desjardins, P.R., Buatois, L.A., Pratt, B.R., Mángano, M.G., 2012. Sedimentological–ichnological model for tide-dominated shelf sandbodies: lower Cambrian Gog Group of western Canada. Sedimentology 59, 1452–1477.
Dieni, I., Massari, F., Médus, J., 2008. Age, depositional environment and stratigraphic value of the Cuccuru'e Flores Conglomerate: insight into the Paleogene to Early Mio- cene geodynamic evolution of Sardinia. Bulletin de la Société Géologique de France 179, 51–72.
Donda, F., Gordini, E., Rebesco, M., Pascucci, V., Fontolan, G., Lazzari, P., Mosetti, R., 2008. Shallow water sea-floor morphologies around Asinara Island (NW Sardinia, Italy). Cont. Shelf Res. 28, 2550–2564.
Ekdale, A.A., Bromley, R.G., Pemberton, S.G., 1984. Ichnology. The Use of Trace Fossils in Sedimentology and Stratigraphy. SEPM Short Course 15 (317 pp.).
Faccenna, C., Speranza, F., D'ajello Caracciolo, F., Mattei, M., Oggiano, G., 2002. Extensional tectonics on Sardinia (Italy): insights into the arc-back-arc transitional regime. Tectonophysics 356, 213–232.
Field, M.E., 1980. Sandbodies on coastal plain shelves: Holocene record of the U.S. Atlantic shelf off Maryland. J. Sediment. Petrol. 50, 505–528.
Flemming, B.W., 2005. Tidal environments. In: Schwartz, M. (Ed.), Encyclopedia of Coastal Science. Springer, Berlin, pp. 1180–1185.
Funedda, A., Oggiano, G., Pasci, S., 1999. Geological map of the Logudoro Basin. Bollettino della Società Geologica Italiana 119, 31–38 (Roma).
Funedda, A., Oggiano, G., Pasci, S., 2000. The Logudoro Basin: a key area for the tectono- sedimentary evolution of North Sardinia. Bollettino della Società Geologica Italiana 119, 31–38.
Funedda, A., Oggiano, G., Pascucci, V., 2003. I depositi miocenici della Sardegna settentrionale: il bacino del Logudoro. Escursione post-congresso. Convegno Geosed 2003, Alghero, 28–30 Settembre 2003, pp. 383–414.
Gawthorpe, R.L., Colella, A., 1990. Tectonic controls on coarse-grained delta depositional systems in rift basins. In: Colella, Prior, D.B. (Eds.), Coarse-grained Deltas. IAS Special 10, pp. 113–127.
Gaynor, G.C., Swift, D.J.P., 1988. Shannon Sandstone depositional model; sand ridge dy- namics on the Campanian Western Interior Shelf. J. Sediment. Res. 58, 868–880.
Gibbs, A.D., 1984. Structural evolution of extensional basin margins. J. Geol. Soc. Lond. 141, 609–620.
Gingras, M.K., Pemberton, S.G., Saunders, T.D.A., 2001. Bathymetry, sediment texture, and substrate cohesiveness: their impact on Glossifungitestrace assemblages at Willapa Bay, Washington. Paleogeography, Paleoclimatology, Paleoecology 169, 1–21.
Grochowski, N.T.L., Collins, M.B., Boxall, S.R., Salomon, J.-C., 1993. Sediment transport predictions for the English Channel, using numerical models. J. Geol. Soc. Lond. 150, 683–695.
Gupta, S., Collier, J.S., Garcia-Moreno, D., Oggioni, F., Trentesaux, A., Vanneste, K., De Batist, M., Camelbeeck, T., Potter, G., Van Vliet-Lanoë, B., Arthur, J.C.R., 2017. Two-stage opening of the Dover Strait and the origin of island Britain. Nat. Commun. 8, 15101. https://doi.org/10.1038/ncomms15101.
Harms, J.C., Southard, J.B., Spearing, D.R., Walker, R.G., 1975. Depositional environments as interpreted from primary sedimentary structures and stratification sequences. SEPM Society for Sedimentary Geology. https://doi.org/10.2110/scn.75.02 short course n. 2.
Harms, J.C., Southard, J.B., Walker, R.G., 1982. Structures and sequences in clastic rocks. SEPM Society for Sedimentary Geology. https://doi.org/10.2110/scn.82.09 short course n. 9.
Harris, P.T., Pattiaratchi, C.B., Collins, M.B., Dalrymple, R.W., 1995. What is a bedload part- ing? In: Flemming, B.W., Bartholoma, A. (Eds.), Tidal Signatures in Modern and An- cient Sediments. 24. IAS Special Publication, pp. 3–18
Hernández-Molina, F.J., Stow, D.A.V., Llave, E., Rebesco, M., Ercilla, G., Van Rooij, D., Mena, A., Vazquez, J.T., Voelker, A.H.L., 2011. Deep-water circulation: processes and prod- ucts (16–18 June 2010, Baiona): introduction and future challenges. Geo-Mar. Lett. 31, 285–300.
Hernández-Molina, F.J., Llave, E., Sierro, F.J., Roque, C., Van der Schee, M., Williams, T., Ledesma, S., Arnais, A., Rosales, C., Brackenridge, R.E., Stow, D.A.V., 2016. Evolution of the Gulf of Cadiz Margin and west Portugal contourite depositional system: tec- tonic, sedimentary and paleoceanographic implications from IODP Expedition 339. Mar. Geol. 377, 7–39.
Johnson, H.D., Baldwin, C.T., 1996. Shallow clastic seas. In: Reading, H.G. (Ed.), Sedimen- tary Environments: Processes, Facies and Stratigraphy. Blackwell Science, Oxford, pp. 232–280.
Jolivet, L., Faccenna, C., 2000. Mediterranean extension and the Africa-Eurasia collision. Tectonics 19, 1095–1106.
Klein, G.D., 1998. Clastic tidalites – a partial retrospective view. In: Alexander, C.R., Davis, R.A., Henry, V.J. (Eds.), Tidalites: Processes and Products. 61. SEPM Special Publica- tion, pp. 5–14.
Kvale, E.P., Archer, A.W., Johnsonn, H.R., 1989. Daily, monthly and yearly tidal cycle within laminated siltstones of the Mansfield Formation (Pennsylvanian) of Indiana. Geology 17, 365–368.
Lanzoni, S., 2000a. Experiments on bar formation in straight flume. 1. Uniform sediment. Water Resour. Res. 36, 3337–3349.
Lanzoni, S., 2000b. Experiments on bar formation in straight flume. 2. Graded sediment. Water Resour. Res. 36, 3351–3363.
Leva-López, J., Rossi, V.M., Olariu, C., Steel, R.J., 2016. Architecture and recognition criteria of ancient shelf ridges; an example from Campanian Almond Formation in Hanna Basin, USA. Sedimentology 63, 1651–1676.
Li, C., O'Donnell, J., 1997. Tidally driven residual circulation in shallow estuaries with lat- eral depth variation. J. Geophys. Res. 102, 915–929.

Li, M.Z., Shaw, J., Todd, B.J., Kostylev, V.E., Wu, Y., 2014. Sediment transport and develop- ment of banner banks and sandwaves in an extreme tidal system: Upper Bay of Fundy, Canada. Cont. Shelf Res. 83, 86–107.
Lim, D.I., Kang, S., Yoo, H.S., Jung, H.S., Choi, J.Y., Kim, H.N., Shin, I.H., 2006. Late Quaternary sediments on the outer shelf of the Korea Strait and their paleoceanographic implica- tions. Geo-Marine Letter 26, 287–296.
Liu, Z.X., Dias, D.X., Berné, S., Yang, W.K., Marsset, T., Tang, Y.X., Bourillet, J.F., 1998. Tidal depositional systems of China's continental shelf, with special reference to the east- ern Bohai Sea. Mar. Geol. 145, 225–268.
Longhitano, S.G., 2008. Sedimentary facies and sequence stratigraphy of coarse-grained Gilbert-type deltas within the Pliocene thrust-top Potenza Basin (Southern Apen- nines, Italy). Sediment. Geol. 210, 87–110.
Longhitano, S.G., 2011. The record of tidal cycles in mixed silici-bioclastic deposits: exam- ples from small Plio-Pleistocene peripheral basins of the microtidal Central Mediter- ranean Sea. Sedimentology 58, 691–719.
Longhitano, S.G., 2013. A facies-based depositional model for ancient and modern, tectonically-confined tidal straits. Terra Nova 25, 446–452.
Longhitano, S.G., 2018a. Between Scylla and Charybdis (part 1): the sedimentary dynam- ics of the modern Messina Strait (central Mediterranean) as analogue to interpret the past. Earth Sci. Rev. 185, 259–287.
Longhitano, S.G., 2018b. Between Scylla and Charybdis (part 2): the sedimentary dynam- ics of the ancient, Early Pleistocene Messina Strait (central Mediterranean) based on its modern analogue. Earth Sci. Rev. 179, 248–286.
Longhitano, S.G., Chiarella, D., 2020. Basic criteria for recognizing ancient tidal straits from the rock record. In: Scarselli, N., Adam, J., Chiarella, D. (Eds.), Regional Geology and Tectonics. MacEachern.
Longhitano, S.G., Nemec, W., 2005. Statistical analysis of bed-thickness variation in a Tortonian succession of biocalcarenitic tidal dunes, Amantea Basin, Calabria, southern Italy. Sediment. Geol. 179, 195–224.
Longhitano, S.G., Steel, R.J., 2016. Deflection of the progradational axis and asymmetry in tidal seaway and strait deltas: insights from two outcrop case studies. In: Hampson, G.J., Reynolds, A.D., Kostic, B., Wells, M.R. (Eds.), Sedimentology of Paralic Reservoirs: Recent Advances. 444. Geological Society, London, Special Publications, pp. 141–172.
Longhitano, S.G., Mellere, D., Steel, R.J., Ainsworth, B.R., 2012a. Tidal depositional systems in the rock record: a review and new insights. In: Longhitano, S.G., Mellere, D., Ainsworth, B. (Eds.), Modern and Ancient Tidal Depositional Systems: Perspectives, Models and Signatures. Sedimentary Geology 279, pp. 2–22.
Longhitano, S.G., Chiarella, D., Di Stefano, A., Messina, C., Sabato, L., Tropeano, M., 2012b. Tidal signatures in Neogene to Quaternary mixed deposits of southern Italy straits and bays. In: Longhitano, S.G., Mellere, D., Ainsworth, B. (Eds.), Modern and Ancient Tidal Depositional Systems: Perspectives, Models and Signatures. Sedimentary Geol- ogy 279, pp. 74–96.
Longhitano, S.G., Chiarella, D., Muto, F., 2014. Three dimensional to two dimensional cross strata transition in the lower Pleistocene Catanzaro tidal strait transgressive succes- sion (southern Italy). Sedimentology 61, 2136–2171.
Longhitano, S.G., Sabato, L., Tropeano, M., Murru, M., Carannante, G., Simone, L., Cilona, A., Vigorito, M., 2015. Outcrop reservoir analogous and porosity changes in continental deposits from an extensional basin: the case study of the upper Oligocene Sardinia Graben System, Italy. Mar. Pet. Geol. 67, 439–459.
Longhitano, S.G., Telesca, D., Pistis, M., 2017. Tidal sedimentation preserved in volcaniclastic deposits filling a peripheral seaway embayment (Early Miocene, Sardinian Graben). In: Longhitano, S.G., Steel, R.J., Pomar, L. (Eds.), Sedimentology in Italy: New Advances and Insights. Marine and Petroleum Geology, Special Issue 87, pp. 31–46.
MacEachern, J.A., Burton, J.A., 2000. Firmground Zoophycos in the Lower Cretaceous Vi- king Formation, Alberta: a distal expression of the Glossifungites Ichnofacies. Palaios 15, 387–398.
MacEachern, J.A., Raychaudhuri, I., Pemberton, S.G., 1992. Stratigraphic applications of the Glossifungites Ichnofacies: delineating discontinuities in the rock record. In: Pemberton, S.G. (Ed.), Applications of Ichnology to Petroleum Exploration. SEPM Core Workshop Notes 17, pp. 169–198.
MacEachern, J.A., Bann, K.L., Bhattacharya, J.P., Howell Jr., C.D., 2005. Ichnology of Deltas: Organism Responses to the Dynamic Interplay of Rivers, Waves, Storms, and Tides. In: Giosan, L., Bhattacharya, J.P. (Eds.), River Deltas–Concepts, Models, and Examples. 83. SEPM Society for Sedimentary Geology, pp. 1–37.
MacEachern, J.A., Dashtgard, S.E., Knaust, D., Catuneanu, O., Bann, K.L., Pemberton, S.G., 2012. Sequence stratigraphy. In: Knaust, D., Bromley, R.G. (Eds.), Trace Fossils as Indi- cators of Sedimentary Environments. Developments in Sedimentology 64. Elsevier, Amsterdam, pp. 157–194.
Martini, I.P., Oggiano, G., Mazzei, R., 1992. Siliciclastic-carbonate sequences of Miocene grabens of Northern Sardinia. Western Mediterranean Sea. Sediment. Geol. 76, 63–78.
Massari, F., Chiocci, F., 2006. Biocalcarenite and mixed cool-water prograding bodies of the Mediterranean Pliocene and Pleistocene: architecture, depositional setting and forcing factors. In: Pedley, H.M., Carannante, G. (Eds.), Cool-Water Carbonates: Depo- sitional Systems and Paleoenvironmental Controls. 255. Geological Society, London, Special Publications, pp. 95–120.
Mazzei, R., Oggiano, G., 1990. Messa in evidenza di due cicli sedimentari nel Miocene dell'area di Florinas (Sardegna settentrionale). Atti della Società Toscana di Scienze Naturali, Memorie 97, 445–459.
Mellere, D., Steel, R.J., 1996. Tidal sedimentation in Inner Hebrides half grabens, Scotland: the Mid-Jurassic Bearreraig Sandstone Formation. In: De Batist, M., Jacobs, P. (Eds.), Geology of Siliciclastic Shelf Seas. 117. Geological Society, London, Special Publica- tions, pp. 49–79.
Messina, C., Nemec, W., Martinius, A.W., Elfenbein, C., 2014. The Garn Formation (Bajocian-Bathonian) in the Kristin Field, Halten Terrace. In: Martinius, A.W., Ravnas, R., Howell, J.A., Steel, R.J., Wonham, J.P. (Eds.), From Depositional Systems to Sedimentary Successions on the Norwegian Continental Margin. 46. IAS Special Publication, pp. 513–550.
Miall, A.D., 1996. The geology of fluvial deposits. Sedimentary Facies, Basin Analysis and Petroleum Geology. 582. Springer, Berlin.
Mitchell, N.C., Huthnance, J.M., Schmitt, T., Todd, B., 2013. Threshold of erosion of submarine bedrock landscapes by tidal currents. Earth Surf. Process. Landf. 38, 627–639.
Murru, M., Bassi, D., Simone, L., 2015. Displaced/reworked rhodolith deposits infilling parts of the complex Miocene multistorey submarine channel: a case history from the Sassari area (Sardinia, Italy). Sediment. Geol. 326, 94–108.
Mutti, E., Nielsen, T.H., 1981. Significance of intraformational rip-up clasts in deep-sea fan deposits. International Association of Sedimentologists, 2nd European Regional Meet- ing, Bologna, 1981, Abstracts, pp. 117–119.
Mutti, E., Tinterri, R., Remacha, E., Mavilla, N., Angella, S., Fava, L., 1999. An introduction to the analysis of ancient turbidite basins from an outcrop perspective. AAPG Course Note 39. https://doi.org/10.1306/CE39687.
Mutti, E., Tinterri, R., Benevelli, G., Biase, D.d., Cavanna, G., 2003. Deltaic, mixed and turbidite sedimentation of ancient foreland basins. Mar. Pet. Geol. 20, 733–755.
Nemec, W., 1990. Aspects of sediment movement on steep delta slopes. In: Colella, A., Prior, D.B. (Eds.), Coarse-Grained Deltas. Blackwell Publishing, Oxford, pp. 29–73.
North, C.P., Davidson, S.K., 2012. Unconfined alluvial flow processes: recognition and in- terpretation of their deposits, and the significance for paleogeographic reconstruc- tions. Earth Sci. Rev. 111, 199–223.
O'Brien, P.E., Wells, A.T., 1986. A small, alluvial crevasse splay. J. Sediment. Petrol. 56, 876–879. Oggiano, G., 1987. La pianura costiera turritana (Sardegna settentrionale), 1:50.000. S.E.L.C.A., Firenze.
Oggiano, G., Pasci, S., Funedda, A., 1995. Il bacino Chivilani-Berchidda: un esempio di struttura transtensiva. Possibili relazioni con la geodinamica cenozoica del Mediterraneo occidentale. Bollettino della Società Geologica Italiana 114, 465–475.
Oggiano, G., Funedda, A., Carmignani, L., Pasci, S., 2009. The Sardinia-Corsica microplate and its role in the Northern Apennine Geodynamics: new insights from the Tertiary intraplate strike-slip tectonics of Sardinia. Ital. J. Geosci. 128, 527–539.

Oggiano, G., Aversano, A., Forci, A., Langiu, M.R., Patta, E.D., Serra, M., 2014. Foglio 459 "Sas- sari". Carta geologica d'Italia in scala 1:50.000. ISPRA, Servizio Geologico d'Italia, Roma.
Olariu, C., Steel, R.J., Dalrymple, R.W., Gingras, M.K., 2012. Tidal dunes v. tidal bars: the sedimentological and architectural characteristics of compound dunes in a tidal sea- way, the lower Baronia Sandstone (Lower Eocene), Ager Basin, Spain. Sediment. Geol. 279, 134–155.
Oudet, J., Münch, P., Borgomano, J., Quillévéré, F., Melinte-Dobrinescu, M., Demory, F., Viseur, S., Cornée, J.-J., 2010. Land and sea study of the northeastern Golfe du Lion rifted margin: the Oligocene-Miocene of southern Provence (Nerthe area, SE France). Bulletin de la Société Géologique de France 181, 591–607.
Park, S.-C., Lee, B.-H., Han, H.-S., Yoo, D.-G., Lee, C.-W., 2006. Late Quaternary stratigraphy and development of tidal sand ridges in the Eastern Yellow Sea. J. Sediment. Res. 76, 1093–1105.
Pasci, S., Oggiano, G., Funedda, A., 1998. Rapporti tra tettonica e sedimentazione lungo le fasce trascorrenti cenozoiche della Sardegna centro-settentrionale. Bollettino della Società Geologica Italiana 117, 443–453.
Peccerillo, A., 2017. Cenozoic volcanism in the Tyrrhenian Sea region. Advances in Volca- nology. Springer, p. 399.
Pemberton, S.G., Frey, R.W., 1985. The Glossifungites Ichnofacies: modern examples from the Georgia coast, U.S.A. In: Curran, H.A. (Ed.), Biogenic Structures: Their Use in Interpreting Depositional Environments. 35. SEPM Special Publication, pp. 237–259.
Pietracaprina, A., 1962. La geologia delle valli del Rio Mascari e Rio Mannu. Studi Sassaresi. Sez. III (X), 1–30.
Pomar, L., Tropeano, M., 2001. The Calcarenite di Gravina Formation in Matera (southern Italy): new insights for coarse-grained, large-scale, cross-bedded bodies encased in offshore deposits. AAPG Bull. 85, 661–689.
Pomar, L., Ward, W.C., 1999. Reservoir-scale heterogeneity in depositional packages and diagenetic patterns on a reef-rimmed platform, Upper Miocene, Mallorca, Spain. AAPG Bull. 83, 1759–1773.
Pomar, L., Brandano, M., Westphal, H., 2004. Environmental factors influencing skeletal grain sediment associations: a critical review of Miocene examples from the western Mediterranean. Sedimentology 51, 627–651.
Postma, G., 1990. Depositional architecture and facies of river and fan deltas: a synthesis. In: Colella, A., Prior, D.B. (Eds.), Coarse-Grained Deltas. Blackwell Publishing Ltd, London, pp. 13–27.
Postma, G., Nemec, W., Kleinspehn, K.L., 1988. Large floating clasts in turbidites: a mech- anism for their emplacement. Sediment. Geol. 58, 47–61.
Pye, K. (Ed.), 1994. Sediment Transport and Depositional Processes. Blackwell Scientific Publications, Oxford, p. 397.
Reading, H.G., Collinson, J.D., 1996. Clastic coasts. In: Reading, H.G. (Ed.), Sedimentary Envi- ronments: Processes, Facies and Stratigraphy. Blackwell Science, Oxford, pp. 154–231.
Reuter, M., Auer, G., Brandano, M., Harzhauser, M., Corda, L., Pillera, W.E., 2017. Post-rift sequence architecture and stratigraphy in the Oligo-Miocene Sardinia Rift (Western Mediterranean Sea). Mar. Pet. Geol. 79, 44–63.
Reynaud, J.-Y., Dalrymple, R.W., 2012. Shallow marine tidal deposits. In: Davis Jr., R.A., Dalrymple, R.W. (Eds.), Principles of Tidal Sedimentology. Springer, New York, pp. 335–370.
Reynaud, J., Tessier, B., Proust, J., Dalrymple, R., Marsset, T., De Batist, M., Bourillet, J., Lericolais, G., 1999. Eustatic and hydrodynamic controls on the architecture of a deep shelf sand bank (Celtic Sea). Sedimentology 46, 703–721.
Reynaud, J.-Y., Vennin, E., Parize, O., Rubino, J.-L., Bourdillon, C., 2012. Incised valleys and tidal seaways: the example of the Miocene Uzès-Castillon basin, SE France. Bulletin de la Société Géologique de France 183 (5), 471–486.
Reynaud, J.-Y., Ferrandini, M., Ferrandini, J., Santiago, M., Thinon, I., André, J.-P., Barthet, Y., Guennoc, P., Tessier, B., 2013. From non-tidal shelf to tide-dominated seaway: the Miocene Bonifacio Basin, southern Corsica. Sedimentology 60, 599–623.
Rossi, V.M., Steel, R.J., 2016. The role of tidal, wave and river currents in the evolution of mixed-energy deltas: example from the Lajas Formation (Argentina). Sedimentology 63, 824–864.
Rossi, V.M., Longhitano, S.G., Mellere, D., Dalrymple, R.W., Steel, R.J., Chiarella, D., Olariu, C., 2017. Interplay of tidal and fluvial processes in an early Pleistocene, delta-fed, strait margin (Calabria, Southern Italy). In: Longhitano, S.G., Steel, R.J., Pomar, L. (Eds.), Sedimentology in Italy: New Advances and Insights. Marine and Petroleum Geology 87, pp. 14–30.
Saito, Y., Katayama, H., Ikehara, K., Kato, Y., Matsumoto, E., Oguri, K., Oda, M., Yumoto, M., 1998. Transgressive and highstand systems tracts and post-glacial transgression, the East China Sea. Sediment. Geol. 122, 217–232.
Santisteban, G., Taberner, C., 1988. Sedimentary models of siliciclastic deposits and coral reefs interrelation. In: Doyle, L.J., Roberts, H.H. (Eds.), Developments in Sedimentol- ogy. 42. Elsevier, Amsterdam, Netherlands, pp. 35–76.
Scasso, R.A., Aberhan, M., Ruiz, L., Weidemeyer, S., Medina, F.A., Kiessling, W., 2012. Inte- grated bio- and lithofacies analysis of coarse-grained, tide-dominated deltaic envi- ronments across the Cretaceous/Paleogene boundary in Patagonia, Argentina. Cretac. Res. 36, 37–57.
Schumm, S.A., 1981. Evolution and response of the fluvial system; sedimentologic impli- cations. In: Ethridge, E.G., Flores, R.M. (Eds.), Recent and ancient non-marine deposi- tional environments. 31. SEPM Special Publication, pp. 19–29.
Seilacher, A., 1967. Bathymetry of trace fossils. Mar. Geol. 5, 413–428.
Simms, A.R., Anderson, J.B., Taha, Z.P., Rodriguez, A.B., 2006. Overfilled versus underfilled incised valleys: examples from the Quaternary Gulf of Mexico incised valleys in time and space. In: Dalrymple, R.W., Leckie, D.A., Tillman, R.W. (Eds.), Incised Valley in Time and Space. 85. SEPM Special Publication, pp. 117–139.
Smith, N.D., Rogers, J. (Eds.), 1999. Fluvial Sedimentology VI. 28. IAS Special Publication (478 p.).
Snedden, J.W., Dalrymple, R.W., 1999. Modern shelf sand ridges: from historical perspec- tive to a unified hydrodynamic and evolutionary model. In: Bergman, K.M., Snedden, J.W. (Eds.), Isolated Shallow Marine Sand Bodies: Sequence Stratigraphic Analysis and Sedimentologic Interpretation. 64. SEPM Special Publication, pp. 13–28.
Sowerbutts, A., Underhill, J.R., 1998. Sedimentary response to intra-arc extension: con- trols on Oligo-Miocene deposition, Sarcidano sub-basin, Sardinia. J. Geol. Soc. Lond. 155, 491–508.
Stow, D.A.V., Hernández-Molina, F.J., Llave, E., Sayago-Gil, M., Díaz-del Río, V., Branson, A., 2009. Bedform-velocity matrix: the estimation of bottom current velocity from bedform observations. Geology 37, 327–330.
Surlyk, F., Noe-Nygaard, N., 1991. Sand bank and dune facies architecture of a wide intracratonic seaway: Late Jurassic–Early Cretaceous Raukelv Formation, Jameson Land, East Greenland. In: Miall, A.D., Tyler, N. (Eds.), The Three-dimensional Facies Architecture of Terrigenous Clastic Sediments and Its Implications for Hydrocarbon Discovery and Recovery. Concepts in Sedimentology and Paleontology 3. SEPM, pp. 261–276.
Suter, J.R., 2006. Facies models revisited: clastic shelves. In: Walker, R.G., Posamentier, H. W. (Eds.), Facies Models Revisited. 84. SEPM Special Publication, pp. 339–397. Swift, D.J.P., 1968. Coastal erosion and transgressive stratigraphy. J. Geol. 76, 444–456.
Swift, D.J.P., Rice, D.D., 1984. Sand bodies on muddy shelves: a model for sedimentation in the western interior cretaceous seaway, North America. In: Tillman, R.D., Seemers, C. T. (Eds.), Siliciclastic Shelf Sediments. 34. SEPM Special Publication, pp. 43–62.
Swift, D.J.P., Phillips, S., Thorne, J.A., 1991. Sedimentation on continental margins, IV: lithofacies and depositional systems. In: Swift, D.J.P., Oertel, G.F., Tillman, R.W., Thorne, J.A. (Eds.), Shelf Sand and Sandstone Bodies: Geometry, Facies and Sequence Stratigraphy. 14. IAS Special Publication, pp. 89–152.
Sztanó, O., de Boer, P., 1995. Basin dimensions and morphology as controls on amplification of tidal motions (the Early Miocene, North Hungarian Bay). Sedimentology 42, 665–682. Taylor, A.M., Goldring, R., 1993. Description and analysis of bioturbation and ichnofabric. J. Geol. Soc. Lond. 150, 141–148.
Taylor, A.M., Goldring, R., Gowland, S., 2003. Analysis and application of ichnofabric. Earth Sci. Rev. 60, 227–259.
Telesca, D., Longhitano, S.G., Pistis, M., Comisso, M.M., Tropeano, M., Sabato, L., 2016. Tidal sedimentation recorded in volcanoclastic deposits filling a peripheral seaway embay- ment (early Miocene, Sardinian Graben System). Rendiconti Online Società Geologica Italiana 40, 536.

Thomas, B., Genneseaux, M., 1986. A two stage rifting in the basin of the Corsica-Sardinia strait. Mar. Geol. 72, 225–239.
Uchman, A., Bubniak, I., Bubniak, A., 2000. Glossifungites Ichnofacies in the area of its no- menclatural archetype, Lviv, Ukraine. Ichnos 7, 183–193.
Vardabasso, S., 1962. Questioni paleogeografiche relative al Terziario antico della Sarde- gna. Mem. Soc. Geol. Ital. 3, 655–673.
Viana, A.R., Faugères, J.-C., Stow, D.A.V., 1998. Bottom-current-controlled sand deposits - a review of modern shallow- to deep-water environments. Sediment. Geol. 115, 53–80.
Vigorito, M., Murru, M., Simone, L., 2006. Architectural patterns in a multistorey mixed carbonate-siliciclastic submarine channel, Porto Torres Basin, Miocene, Sardinia, Italy. Sediment. Geol. 186, 213–236.
Walker, R.G., 1984. Shelf and shallow marine sands. In: Walker, R.G. (Ed.), Facies Models. Geoscience Canada, Reprint Series 1, pp. 141–170.
Walker, R.G., James, N.P. (Eds.), 1992. Facies Models, Response to Sea Level Changes. Geological Association of Canada (454 p.).
Wang, Y., Zhang, Y., Zou, X., Zhu, D., Piper, D., 2012. The sand ridge field of the South Yel- low Sea: origin by river-sea interaction. Mar. Geol. 291, 132–146.
Weise, B.R., 1980. Wave-dominated Delta Systems of the Upper Cretaceous San Miguel Formation, Maverick Basin, South Texas. Report of Investigations 107. Bureau of Eco- nomic Geology, Austin, TX (33 p.).
Wells, M., Allison, P., Piggott, M., Hampson, G., Pain, C., Gorman, G., 2010a. Tidal modeling of an ancient tide-dominated seaway, part 1: model validation and application to global early Cretaceous (Aptian) tides. J. Sediment. Res. 80 (393), 410.
Wells, M.R., Allison, P.A., Piggott, M.D., Hampson, G.J., Pain, C.C., Gorman, G.J., 2010b. Tidal modelling of an ancient tide-dominated seaway, part 2: the Aptian Lower Greensand Seaway of northeast Europe. J. Sediment. Res. 80, 411–439.
Willis, B.J., 2005. Deposits of tide-influenced river deltas. In: Giosan, L., Bhattacharya, J.P. (Eds.), River Deltas –Concepts, Models and Examples. 83. SEPM Special Publication, pp. 87–129.
Zaitlin, B.A., Dalrymple, R.W., Boyd, R., 1994. The stratigraphic organization of incised-val- ley systems associated with relative sea-level change. In: Dalrymple, R.W., Boyd, R., Zaitlin, B.A. (Eds.), Incised-Valley Systems: Origin and Sedimentary Sequences. 51. SEPM, Special Publication, pp. 45–60.

Figure Captions

Fig. 1. (A) General geological sketch of Sardinia in the central Mediterranean regional-scale framework (inset), with the indication of the study area. In yellow, the Oligo-Miocene sedimentary deposits filling the Sardinian Graben System are highlighted. (B) Geology of the Porto Torres (PTB) and Logudoro (LB) basins. In this latter, the main outcrop localities cited in the text are indicated. (C) Palaeogeographic regional frameworks of the Sardinian-Corsica block at the Serravallian (modified after Dercourt et al., 2000; Jolivet and Faccenna, 2000; Barrier and Vrielynck, 2008; Cherchi et al., 2008; Reynaud et al., 2012), showing the main stages of inferred oceanographic connections of the Sardinian Seaway and consequent current-dominated dynamics. (D) Reconstruction of the Sardinian Seaway during the Miocene (modified, after Longhitano et al., 2017). The indicated locations refer to exposed tidalite-bearing successions of different ages, indicating stages of opening of the seaway during the Miocene. (For interpretation of the references to color in this figure legend, the reader is referred to the web version of this article.)

Fig. 2. (A) Detailed geological map of the study area showing the location of the measured sedimentological logs. (B) Stratigraphic columns showing the study succession. (C) Geological cross sections, with the indication of the main sediment transport directions inferred from large-scale cross bedding.

Fig. 3. Sedimentological logs measured in the study area (see inset for location). For facies code abbreviations and descriptions, refer to Table 1.

Fig. 4. Outcrop photographs showing sedimentological features of Facies association A. (A) Vertical stacking of sub-facies A1a and A1b separated by an irregular erosional surface. Facies A3 rests erosionally on both Facies A2 and A1. (B) Detail of the textural features of sub-facies A1a. (C) Co-sets separated by internal discontinuities are characteristic of Facies A1. (D) Deposits of Facies A2. Note erosional bases, fining-upward trends and tabular bed geometry. (E) Internal cross bedding in the deposits of sub-facies A2a (arrows indicate vertically-oriented burrows). (F) Detail from the previous photograph showing Glossifungites. (G) Outcrop photograph of the erosional surface separating the deposits of sub-facies A2b and the overlying Facies A3. (H, I) Details from the previous outcrop, showing polygenic sub-rounded pebbles and cobbles, concentrated at the base of the sequence and scattered throughout the bed (arrows indicate mudstone intra-clasts). (J) Deposits of Facies A3 showing north-trending foreset cross stratification (arrows indicate conglomerates, at the bases of the strata, imitating channel lags). (K, L) Mudstone clasts and coal fragments are also present.

Fig. 5. Outcrop photographs of Facies association B near Florinas, interpreted as deltaic deposits. (A) Panoramic view of the active quarry, where the uppermost erosional contact separating the underlying 'Sabbie di Florinas' Fm and the overlying CS deposits (uppermost sequence) is indicated. (B) Detailed views of different quarry fronts reveal large-scale foreset bedding of Facies B1, belonging to two vertically-stacked deltaic units, the lowermost of which contains a 25-m-thick slump intercalation (see line-drawing in C).

Fig. 6. (A) Photo-panel from the Florinas Quarry (see location in Fig. 5A) showing foreset architectures of Facies B1 and the erosional contact with the overlying deposits of Facies CS. (B) Detail of offlap break point (white arrow) separating topset from foreset geometries. (C) Alternating deposits of sub-facies B1a and B1b are visible along the foreset beds. (D) Anomalously thick fine-grained intervals with loading and scouring structures in the foreset beds. (E) Details of sub-facies B1a from the previous outcrop showing close-up textural features (coin as scale is 2 cm diameter). (F) Details of sub-facies B1a displaying inverse-graded cross beds with erosional bases and bipartite grain size zones. (G) Details of normal- graded cross beds with erosional bases and grain size differences are visible in the deposits of sub-facies B1a.

Fig. 7. Outcrop photographs of sub-facies B2a near Ploaghe showing different ordering of cross bedding. (A) 1st-order discontinuities form tabular sand bodies, here deformed due to the activity of a marginal fault on the left side of the picture. Note internal small-scale foresets. (B) 2nd-order cross bedding visible along a road cut. (C) Tabular cross beds with angular foresets migrating perpendicularly respect to the progradational direction (towards the observer) in a delta-platform environment. (D) 3rd-order cross bedding including (E, F) up-dip migrating internal 4th-order foresets. (G) Macroscopic textural features of sediments of sub-facies B2a and (H, I) microscopic features seen from thin sections observed at plane-polarised light and cross-polarised light respectively (Afs = Alkali feldspar; Qtz = Quartz; CalC = Calcite Cement; Pl = Plagioclase). Note alkali feldspars weathered in clay minerals, and the coexistence of at least two generations of plagioclase, indicating sediment recycling. (J, K) Micro-photograph showing weathered plagioclase. (L) Burrowing visible on a bed surface.

Fig. 8. (A) Inferred 3D reconstruction proposed for the submerged deltaic depositional setting of Facies association B. (B) Facies B1 record delta slope deposits, including gravity dominated and current influenced sandstone and located along a delta slope environment. (C) Facies B2 accumulated in a current-dominated/wave-influenced delta-platform environment, where large-scale bedforms migrated perpendicularly respect to the delta progradational axis, with superimposed minor smaller bedforms accreting on the top surfaces. Both the environments were subject to alongshore currents having different impact on the sedimentation depending on depth differences.

Fig. 9. Outcrop photographs of Facies association C. (A) Photomosaic and corresponding line-drawing of the section exposed W-SW of Ploaghe, showing the erosional contact (tr1) separating the underlying facies association B from the overlying association C. (B) A correlative erosional surface (tr1) separating facies association B and C is visible near Florinas. (C) Coarsening-to-fining-grain-size intervals, referable to neap-spring tidal cycles, are visible at close-up view in the sub-facies C1a, also including vertical burrows (S = Skolithos sp.). (D) Herringbone bi-directional ripples observable at the top of the sub-facies C1a succession, below the upward transition with the biocalcarenites of sub-facies C1b.

Fig. 10. (A) Outcrop showing the truncation surface (tr2) at the C1a-C1b boundary. Note gutter casts (arrows) and diffuse cross bedding. (B, C) Details of the Skolithos sp. visible within the C1b deposits. (D) Shell patches (mostly ostreiids, but also including echinoids and algae) filling the irregularities at the tr2 basal contact. (E) Detail showing the mixed composition containing dominant bioclasts and interspersed quartz grains and lava fragments (dark). (F) Additional outcrop detail of sub-facies C1b. Gutter casts (arrows) (G) are also present within the deposits, pointing out the occurrence of internal discontinuities of probable erosional origin.

Fig. 11. (A) Aerial photograph of the bioclastic ridge (Facies C2) exposed near Mores. Note the high angle difference between master bedding and superimposed minor foresets. (B, C) Cross-sectional views of the Mores ridge. It lies erosionally onto the Facies Association B deposits and contains a variety of cross bedding of different rank and orientation (see rose diagram). (D) Detail of sub-facies C2a with (E) Thalassinoides burrows. (F) Large-scale, 1st-order bedding (N130°E) visible in a cross-sectional view is oriented perpendicularly with respect the elongation axis of the Mores ridge (N220°E). Note small-scale foresets (N189–330°E) reflecting minor superimposed bedforms (dunes?).

Fig. 12. (A) Panoramic view of the top of Mt. Santo section, where the deposits belonging to Facies Association C are overlain by Quaternary lava flows. Carbonates of sub-facies C2b occur as lenticular intercalations showing internal clinoform architectures (B). Close-up view of a portion of the outcrop in (A) showing a clinoform prograding towards E-NE and suggesting lateral migration of an individual ridge, as in the inset. (C) Close-up view of the bottomset, showing low-angle cross-stratified cosets. (D) Close-up view of the bottomset, which include normally graded strata, with tabular, lenticular and sigmoidal shapes. Single strata hold indistinct foresets, dipping in the opposite direction compared to the master bedding

(black arrows). (E) Photomicrograph of sub-facies C2b showing its main textural features and bioclastic content. Benthic Foraminifera (rotaliinids) (BF) and fragments of rhodolith nodule (RN). (F) Rotaliinid larger Foraminifera (BF), fragments of textulariids (T) and of Echinoid plates (EC). The background consists of small bioclasts, calcite cement and clay matrix.

Fig. 13. (A) Additional aerial view of S-SW-migrating carbonate ridges exposed near Ploaghe (note high angle between master bedding and lateral accretion). (B) They appear elongate and include at least three accretional sub-units that reflect stages of active migration interrupted by momentary pauses. Rose diagrams show the southwest migration. (C) Facies detail from one of the previous ridge. (D–F) Thin-section features showing algal nodules, benthic foraminifera (rotaliniids and textulariids) in a carbonate matrix and sparite (BF = benthic foraminifera; T = textulariids; RN = rhodolith nodule).

Fig. 14. Palaeogeographic reconstruction of the Logudoro Basin (LB) and the Porto Torres Basin (PT) from the middle-Burdigalian to the Messinian. (A) During the deposition of the 1st depositional sequence, the Logudoro Basin was probably formed by at least two main depocenters hosting lacustrine-deltaic sedimentation. (B) In a successive stage, marine waters invaded the basin from the NW, turning it into a S-SE-trending large embayment with shelf deposits. (C) After a dramatic phase of uplift and consequent subaerial exposure/erosion, (D) fluvial-to-shallow marine deposits (Facies association A) restored late-LST-early-TST shallow-marine sedimentation. (E) The late Serravallian is the time when an oceanographic opening occurred in the Logudoro Basin with the possible connection with adjacent basins (Facies association B) and the onset of a seaway circulation. (F) A late stage of transgression imparted to the basin a tidal hydrodynamics with the promotion of actively migrating carbonate sand ridges and dunes (Facies association C).

Fig. 15. Block-diagram reconstruction of the Logudoro Basin interpreted as a branch of the larger Sardinian Seaway during the Serravallian-Tortonian. The location of the major tidal sand ridge is reported, as well as the inferred direction of flood/ebb currents.

Fig. 16. Semi-regional scale correlation based on the occurrence of large-scale (tidal?) cross-bedding observed in sand bodies scattered across the Sardinian Graben System, inferring momentary phases of active open-marine circulation that characterised the Sardinian Seaway during the Miocene.

Table 1
List of the facies associations recognised in the present work, including description and interpretation of depositional processes, environments and systems.

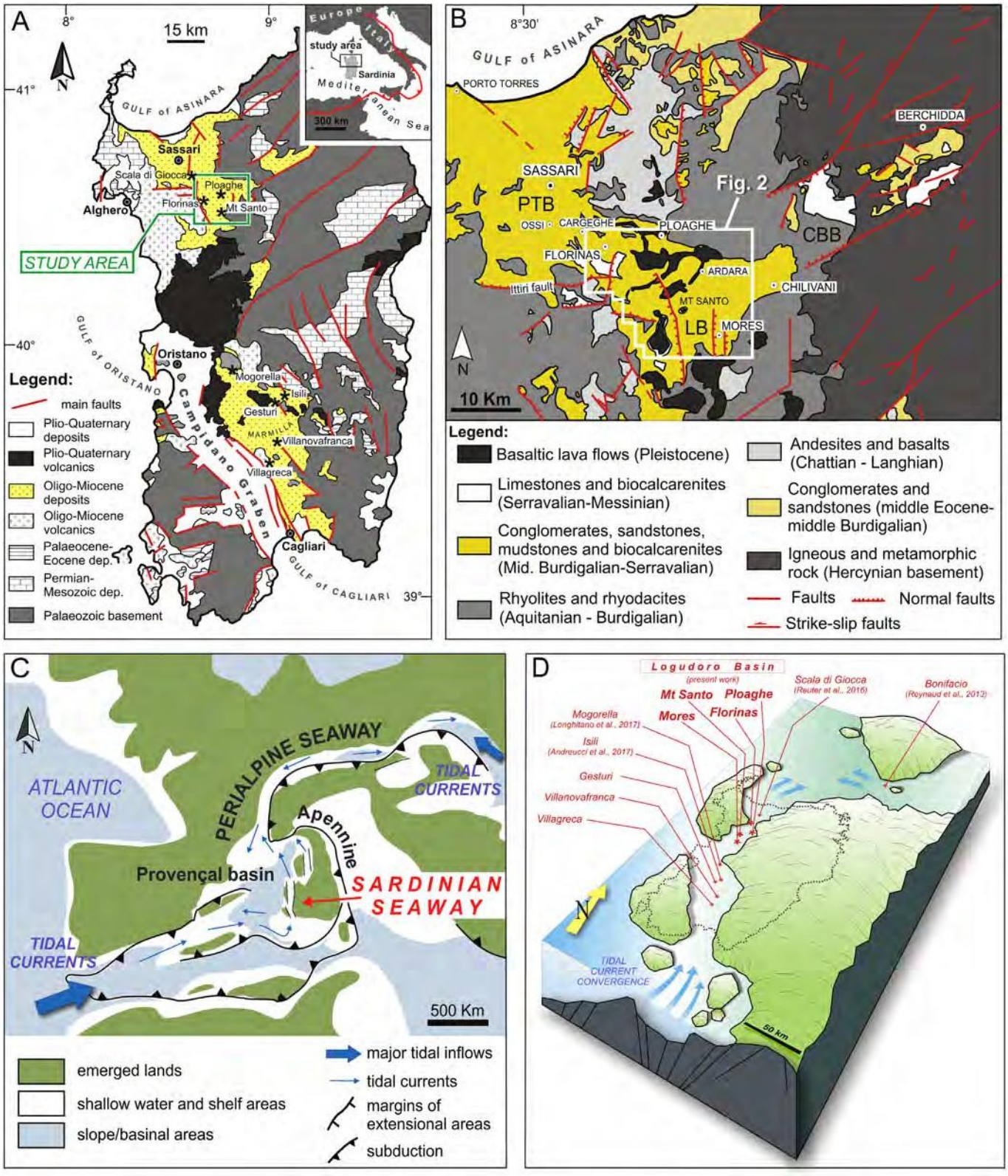
A
15 km
8°
9°
41°
40°
39°
N
GULF of ASINARA
GULF of ORISTANO
GULF of CAGLIARI
Europe
Italy
study area
Sardinia
Mediterranean Sea
300 km
Sassari
Scala di Giocca
Ploaghe
Florinas
Mt Santo
Alghero
STUDY AREA
Oristano
Mogorella
Isili
Gesturi
MARMILLA
Villanovafranca
Villagreca
Campidano Graben
Cagliari
Legend:
main faults
Plio-Quaternary deposits
Plio-Quaternary volcanics
Oligo-Miocene deposits
Oligo-Miocene volcanics
Palaeocene-Eocene dep.
Permian-Mesozoic dep.
Palaeozoic basement
B
8°30'
GULF of ASINARA
PORTO TORRES
BERCHIDDA
SASSARI
PTB
Fig. 2
OSSI
CARGEGHE
PLOAGHE
CBB
FLORINAS
ARDARA
CHILIVANI
Ittiri fault
MT SANTO
LB
MORES
N
10 Km
Legend:
Basaltic lava flows (Pleistocene)
Limestones and biocalcarenites (Serravalian-Messinian)
Conglomerates, sandstones, mudstones and biocalcarenites (Mid. Burdigalian-Serravalian)
Rhyolites and rhyodacites (Aquitanian - Burdigalian)
Andesites and basalts (Chattian - Langhian)
Conglomerates and sandstones (middle Eocene-middle Burdigalian)
Igneous and metamorphic rock (Hercynian basement)
Faults
Normal faults
Strike-slip faults
C
N
ATLANTIC OCEAN
PERIALPINE SEAWAY
TIDAL CURRENTS
Apennine
Provençal basin
SARDINIAN SEAWAY
TIDAL CURRENTS
500 Km
emerged lands
shallow water and shelf areas
slope/basinal areas
major tidal inflows
tidal currents
margins of extensional areas
subduction
D
Logudoro Basin
(present work)
Mt Santo
Ploaghe
Mores
Florinas
Scala di Giocca
(Reuter et al., 2016)
Bonifacio
(Reynaud et al., 2012)
Mogorella
(Longhitano et al., 2017)
Isili
(Andreucci et al., 2017)
Gesturi
Villanovafranca
Villagreca
N
TIDAL CURRENT CONVERGENCE
50 km

Fig. 1.

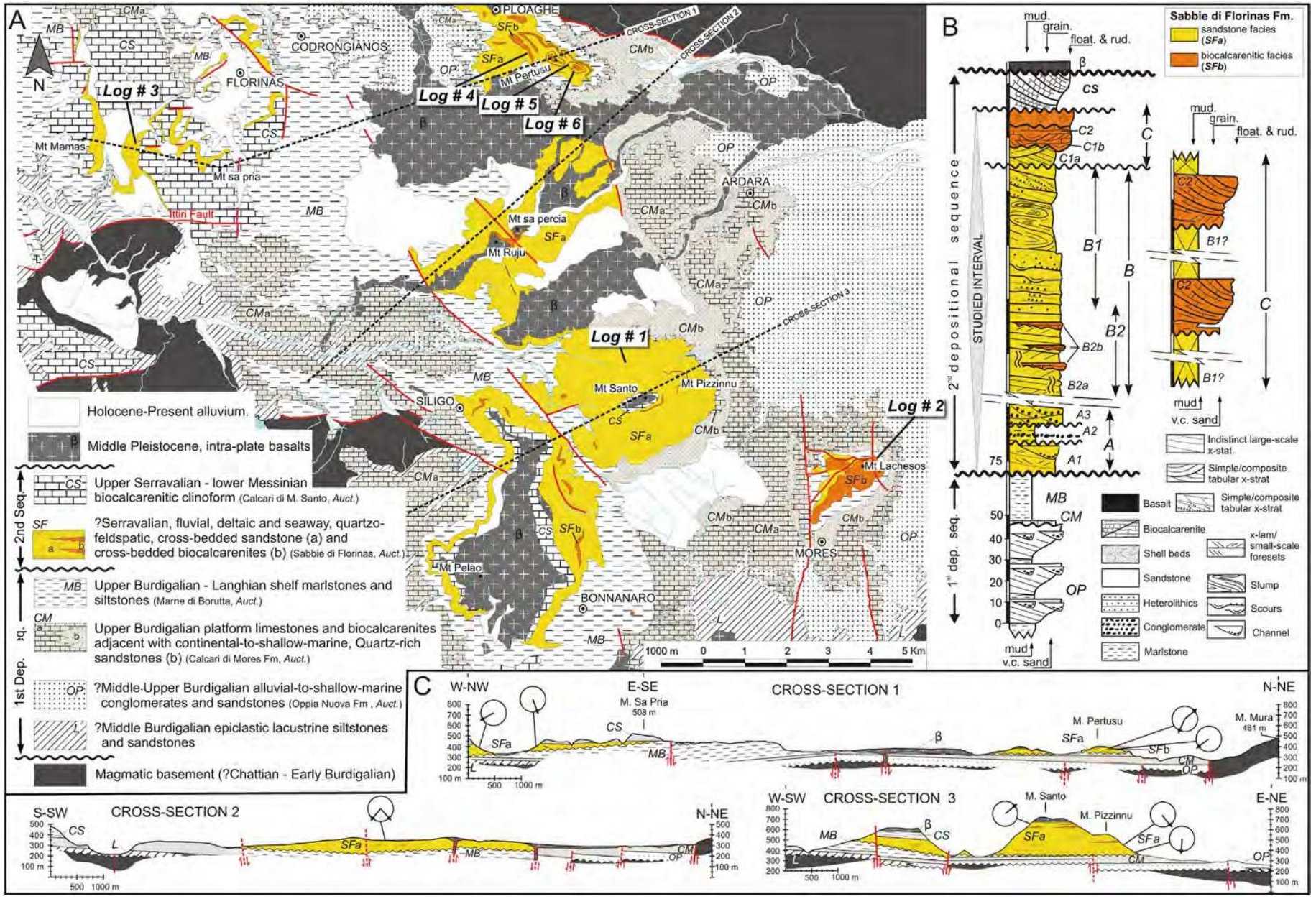
A
B
C
N
PLOAGHE
CODRONGIANOS
FLORINAS
ARDARA
SILIGO
BONNANARO
MORES
Mt Mamas
Mt sa pria
Mt Pertusu
Mt sa percia
Mt Ruju
Mt Santo
Mt Pizzinnu
Mt Lachesos
Mt Pelao
Ittiri Fault
Log # 1
Log # 2
Log # 3
Log # 4
Log # 5
Log # 6
CROSS-SECTION 1
CROSS-SECTION 2
CROSS-SECTION 3
Holocene-Present alluvium.
Middle Pleistocene, intra-plate basalts
Upper Serravalian - lower Messinian biocalcarenitic clinoform (Calcari di M. Santo, Auct.)
?Serravalian, fluvial, deltaic and seaway, quartzo-feldspatic, cross-bedded sandstone (a) and cross-bedded biocalcarenites (b) (Sabbie di Florinas, Auct.)
Upper Burdigalian - Langhian shelf marlstones and siltstones (Marne di Borutta, Auct.)
Upper Burdigalian platform limestones and biocalcarenites adjacent with continental-to-shallow-marine, Quartz-rich sandstones (b) (Calcari di Mores Fm, Auct.)
?Middle-Upper Burdigalian alluvial-to-shallow-marine conglomerates and sandstones (Oppia Nuova Fm , Auct.)
?Middle Burdigalian epiclastic lacustrine siltstones and sandstones
Magmatic basement (?Chattian - Early Burdigalian)
2nd Seq.
1st Dep. Seq.
Sabbie di Florinas Fm.
sandstone facies (SFa)
biocalcarenitic facies (SFb)
STUDIED INTERVAL
2nd depositional sequence
1st dep. seq.
mud.
grain.
float. & rud.
mud
v.c. sand
Indistinct large-scale x-strat.
Simple/composite tabular x-strat
Basalt
Biocalcarenite
Shell beds
Sandstone
Heterolithics
Conglomerate
Marlstone
x-lam/ small-scale foresets
Slump
Scours
Channel
W-NW
E-SE
N-NE
S-SW
W-SW
E-NE
M. Sa Pria
508 m
M. Pertusu
M. Mura
481 m
M. Santo
M. Pizzinnu
1000 m 0 1 2 3 4 5 Km

Fig. 2.

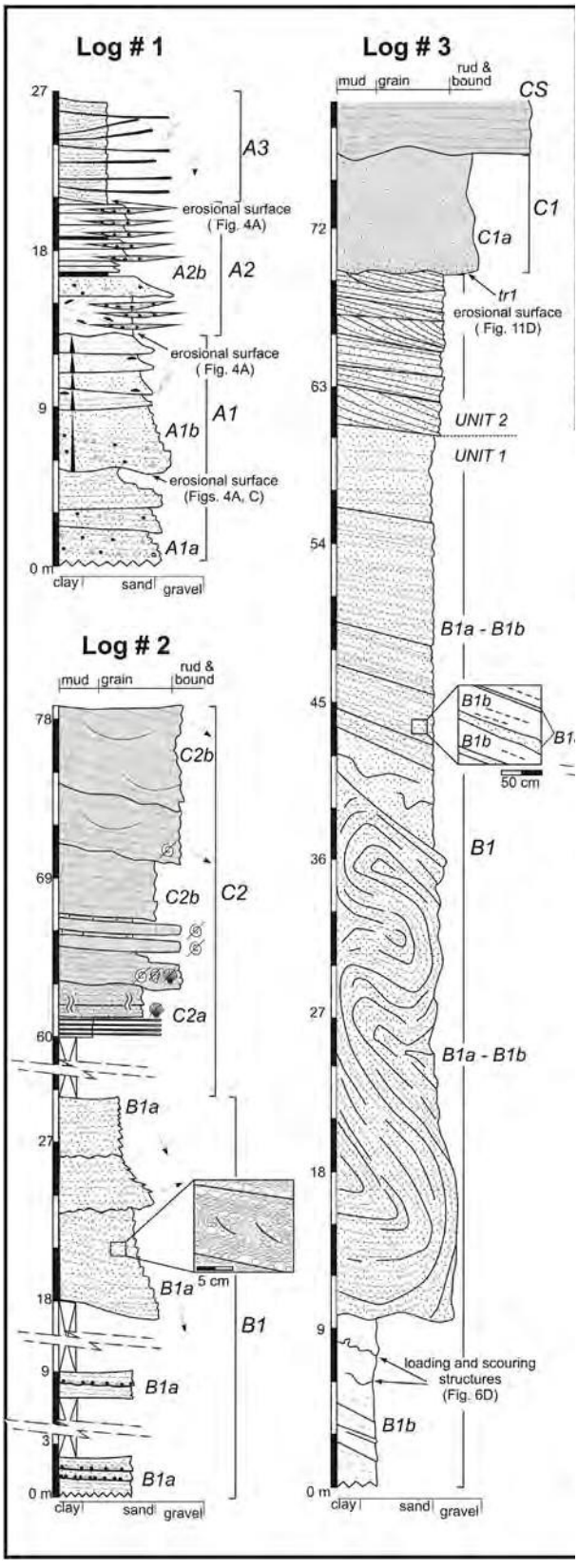
Log # 1
27
18
9
0 m
A3
erosional surface
(Fig. 4A)
A2b
A2
erosional surface
(Fig. 4A)
A1b
A1
erosional surface
(Figs. 4A, C)
A1a
clay
sand
gravel
Log # 2
mud
grain
rud &
bound
78
69
60
27
18
9
3
0 m
C2b
C2b
C2
C2a
B1a
5 cm
B1a
B1
B1a
B1a
clay
sand
gravel
Log # 3
mud
grain
rud &
bound
72
63
54
45
36
27
18
9
0 m
CS
C1
C1a
tr1
erosional surface
(Fig. 11D)
UNIT 2
UNIT 1
B1a - B1b
B1b
B1b
50 cm
B1
B1a - B1b
loading and scouring
structures
(Fig. 6D)
B1b
clay
sand
gravel

Fig. 3

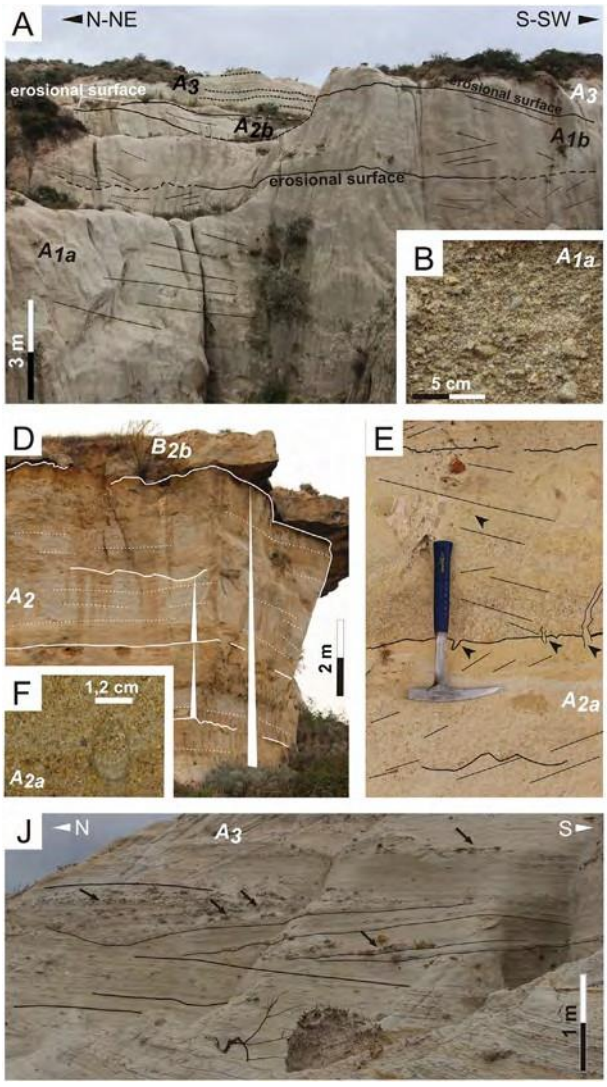
A
N-NE
S-SW
erosional surface
A3
A2b
erosional surface
A3
A1b
erosional surface
A1a
3 m
B
A1a
5 cm
D
B2b
A2
2 m
F
1,2 cm
A2a
E
A2a
J
N
A3
S
1 m

F

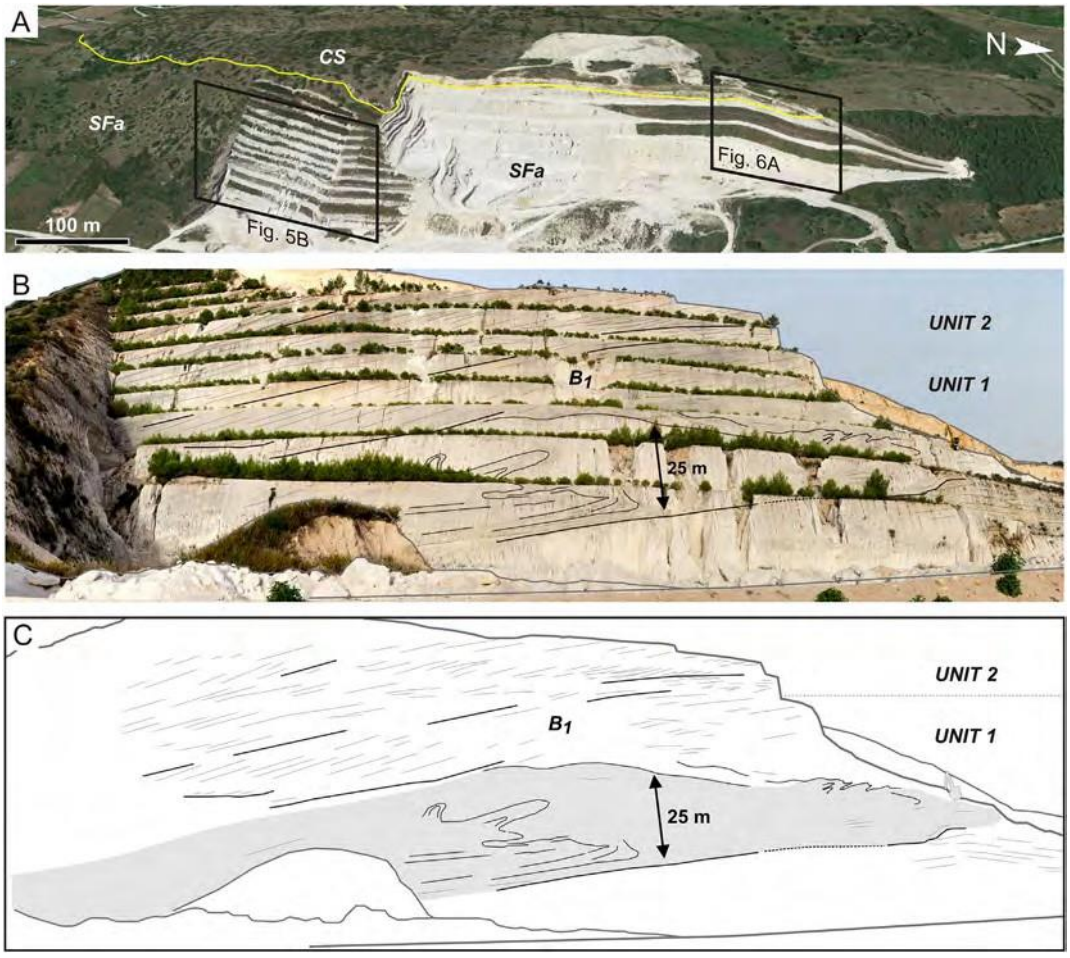
A
CS
N
SFa
SFa
Fig. 6A
Fig. 5B
100 m
B
UNIT 2
UNIT 1
B1
25 m
C
UNIT 2
UNIT 1
B1
25 m

Fig. 5

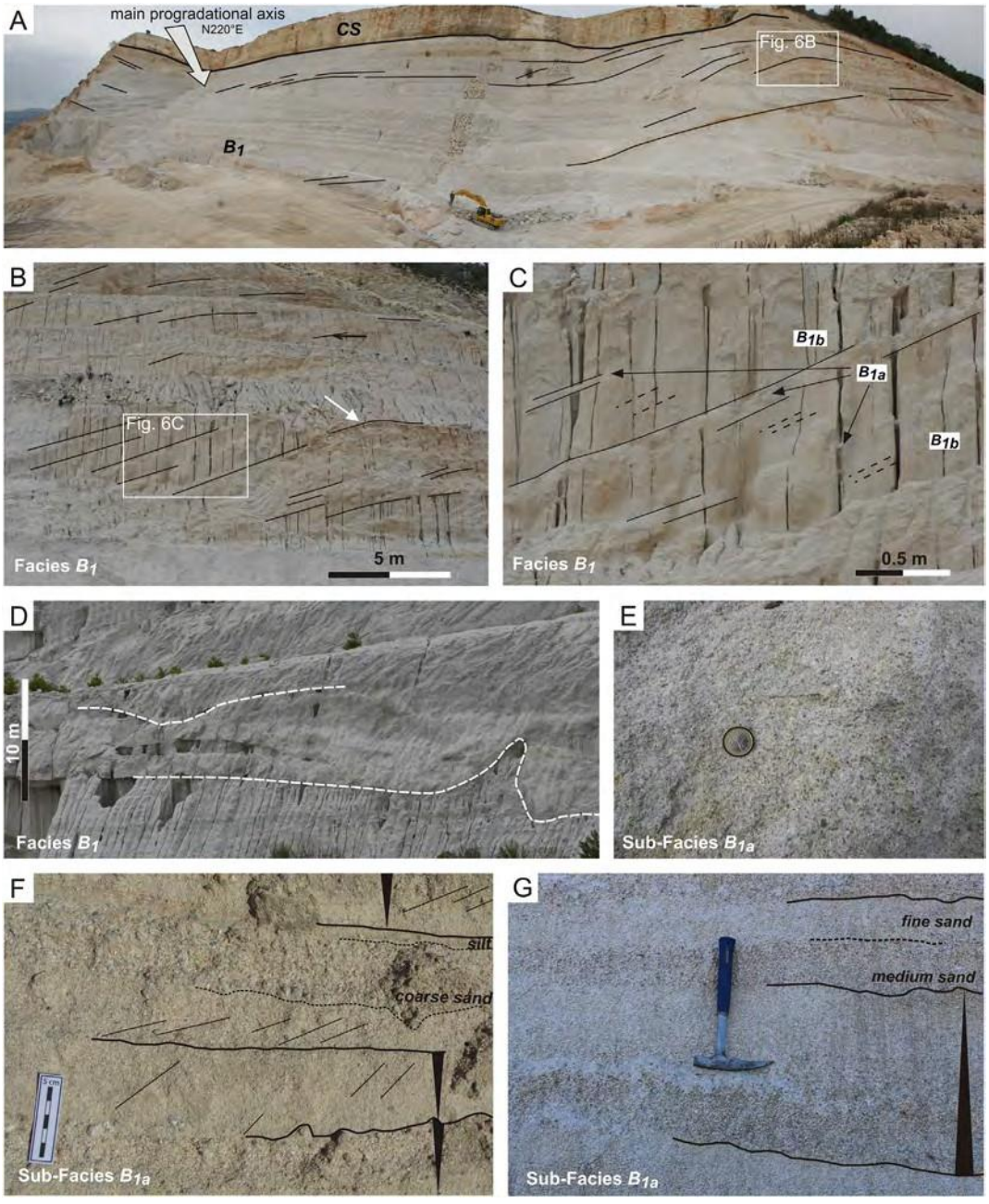
A
main progradational axis
N220°E
CS
Fig. 6B
B1
B
Fig. 6C
Facies B1
5 m
C
B1b
B1a
B1b
Facies B1
0.5 m
D
10 m
Facies B1
E
Sub-Facies B1a
F
silt
coarse sand
Sub-Facies B1a
G
fine sand
medium sand
Sub-Facies B1a

Fig. 6

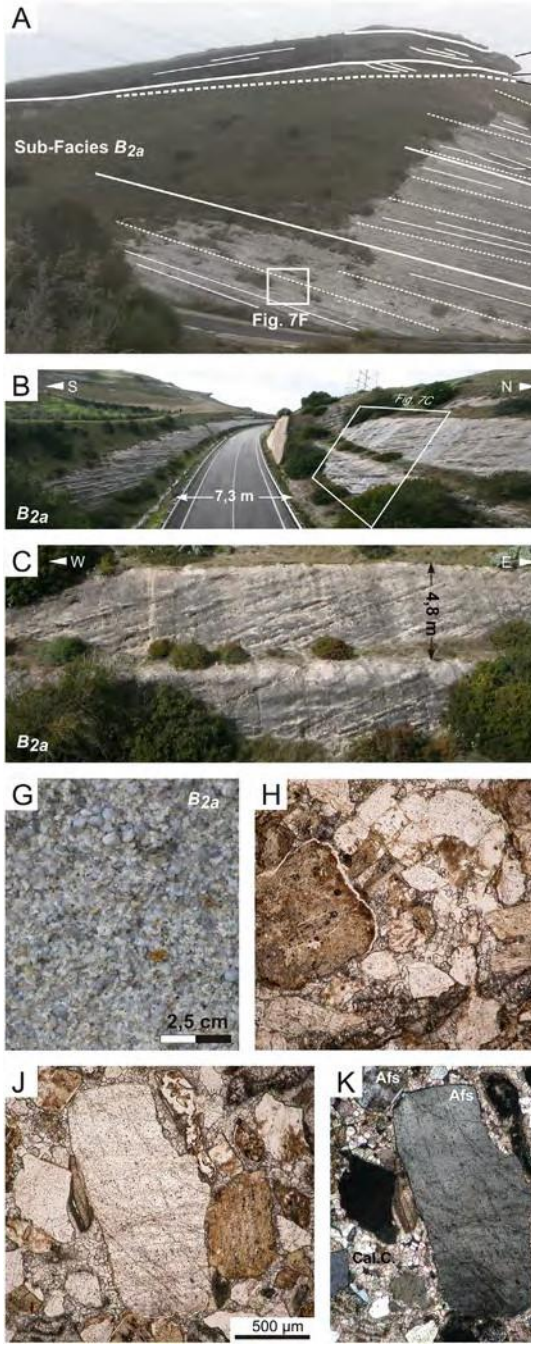
A
Sub-Facies B_{2a}
Fig. 7F
B
S
N
Fig. 7C
7,3 m
B_{2a}
C
W
E
4,8 m
B_{2a}
G
B_{2a}
2,5 cm
H
J
500 µm
K
Afs
Afs
Cal.C.

Fig. 7

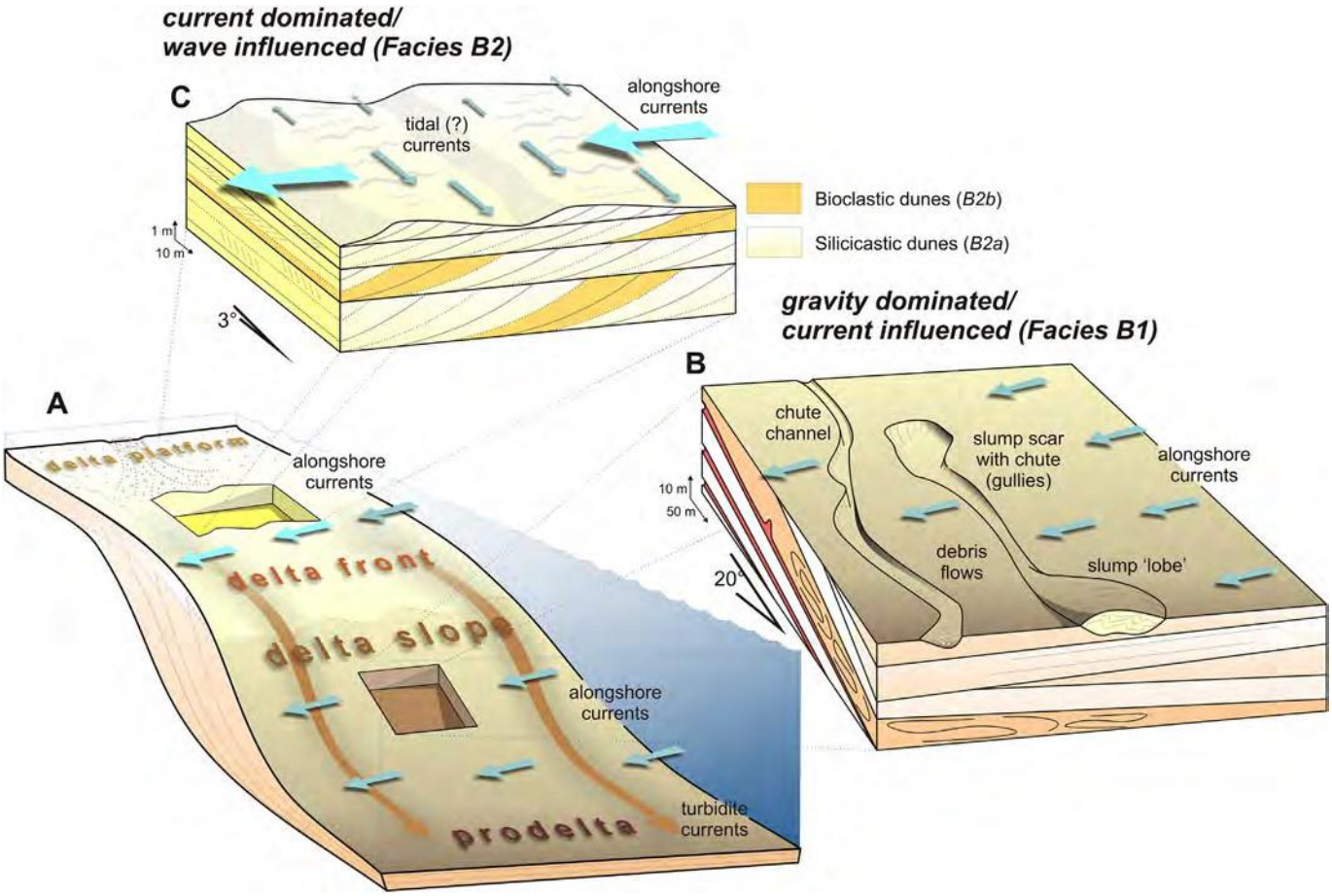
current dominated/
wave influenced (Facies B2)
C
alongshore
currents
tidal (?)
currents
1 m
10 m
3°
Bioclastic dunes (B2b)
Silicicastic dunes (B2a)
gravity dominated/
current influenced (Facies B1)
B
chute
channel
slump scar
with chute
(gullies)
alongshore
currents
10 m
50 m
20°
debris
flows
slump 'lobe'
A
delta platform
alongshore
currents
delta front
delta slope
alongshore
currents
prodelta
turbidite
currents

Fig. 8

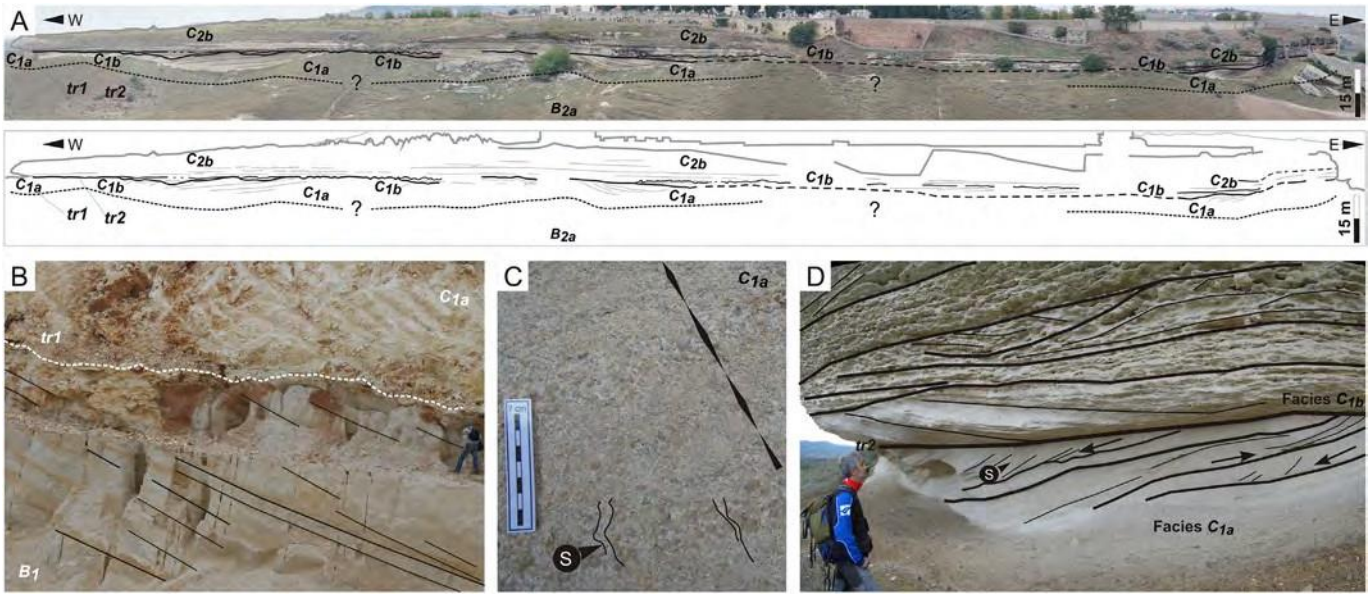
A
W
E
C2b
C1a
C1b
tr1
tr2
?
B2a
15 m
B
C1a
tr1
B1
C
S
D
Facies C1b
Facies C1a

Fig. 9

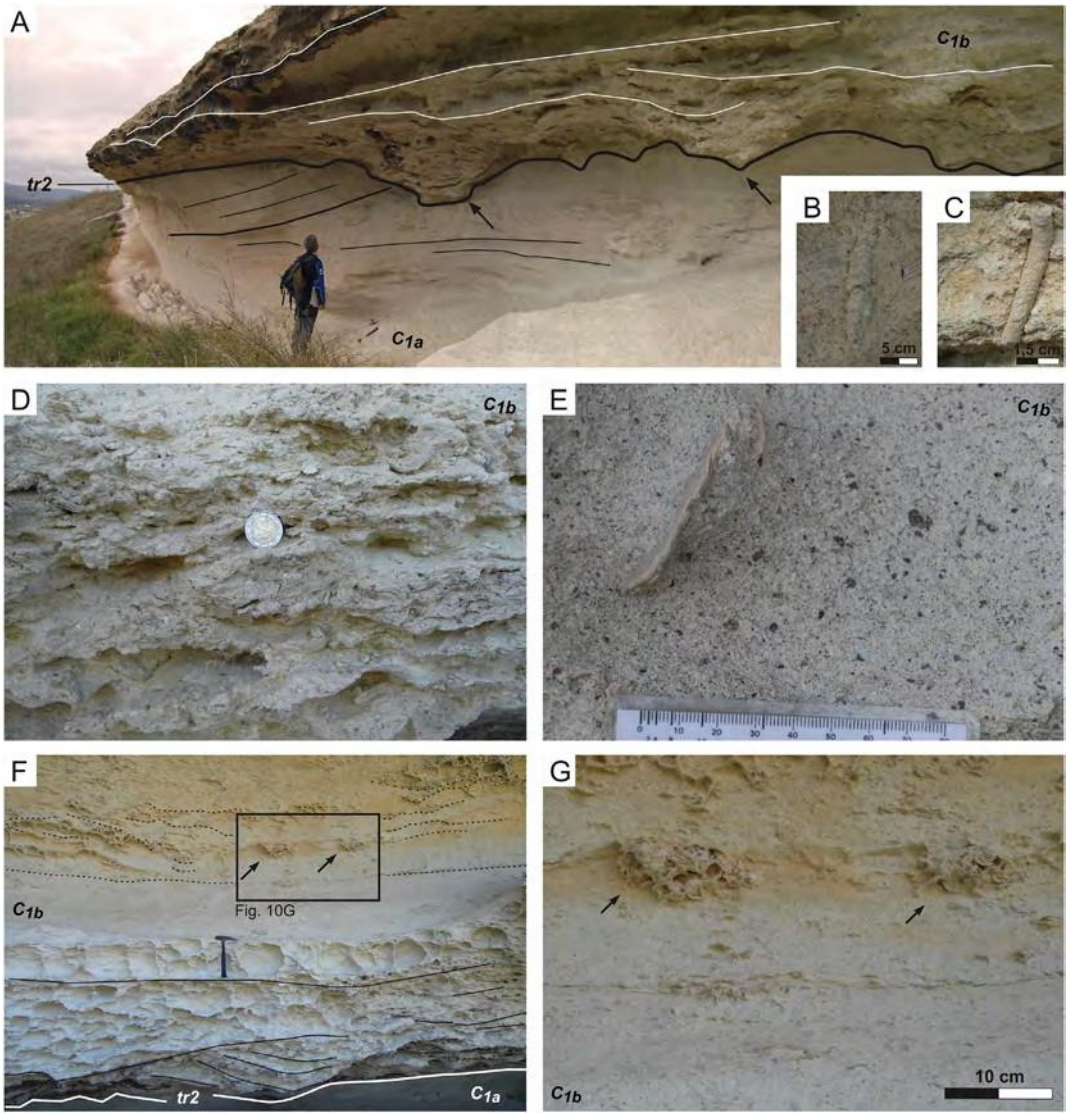
A
C1b
tr2
C1a
B
5 cm
C
1.5 cm
D
C1b
E
C1b
F
C1b
Fig. 10G
tr2
C1a
G
C1b
10 cm

Fig. 10

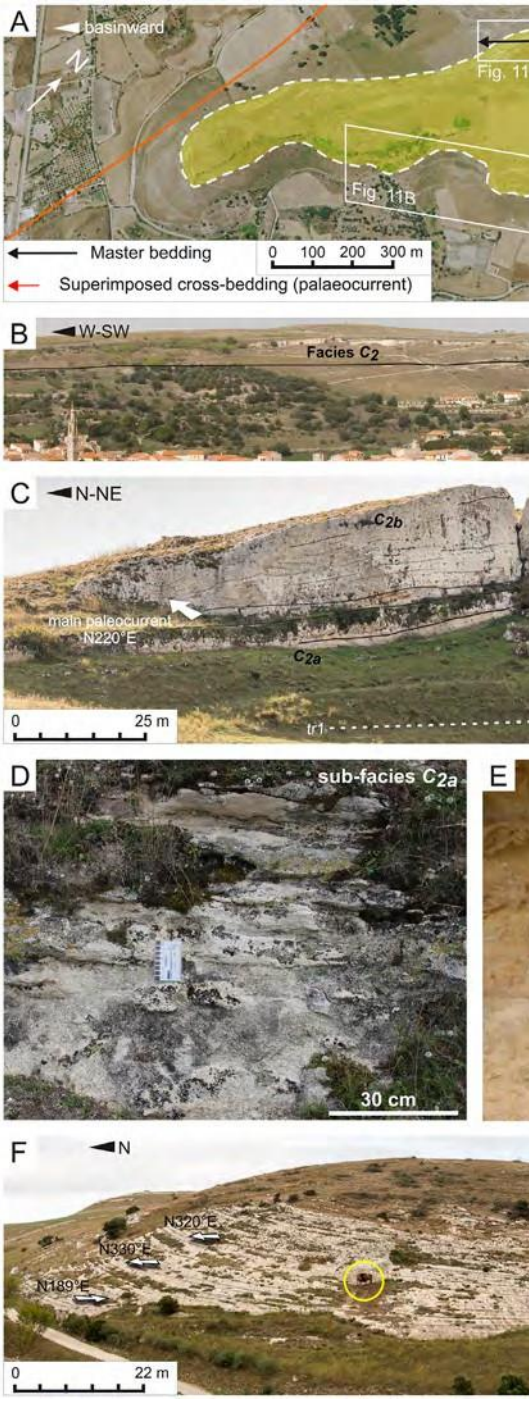
A
basinward
N
Fig. 11
Fig. 11B
Master bedding
0 100 200 300 m
Superimposed cross-bedding (palaeocurrent)
B
W-SW
Facies C2
C
N-NE
C2b
main paleocurrent
N220°E
C2a
0 25 m
tr1
D
sub-facies C2a
30 cm
E
F
N
N320°E
N330°E
N189°E
0 22 m

Fig. 11

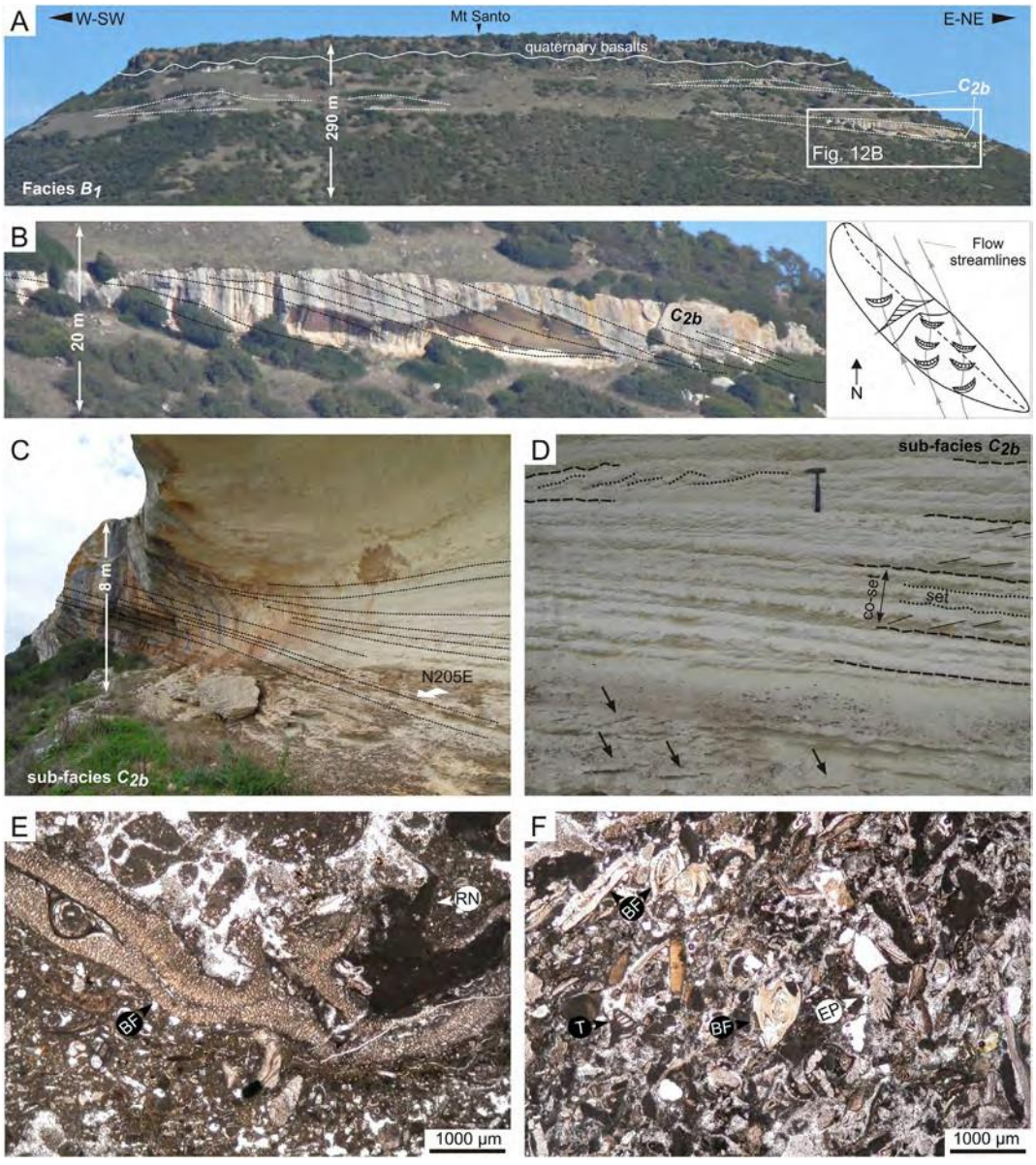
A
W-SW
Mt Santo
E-NE
quaternary basalts
290 m
C_{2b}
Fig. 12B
Facies B_1
B
20 m
C_{2b}
Flow streamlines
N
C
8 m
N205E
sub-facies C_{2b}
D
sub-facies C_{2b}
co-set
set
E
RN
BF
1000 µm
F
BF
T
BF
EP
1000 µm

Fig. 12

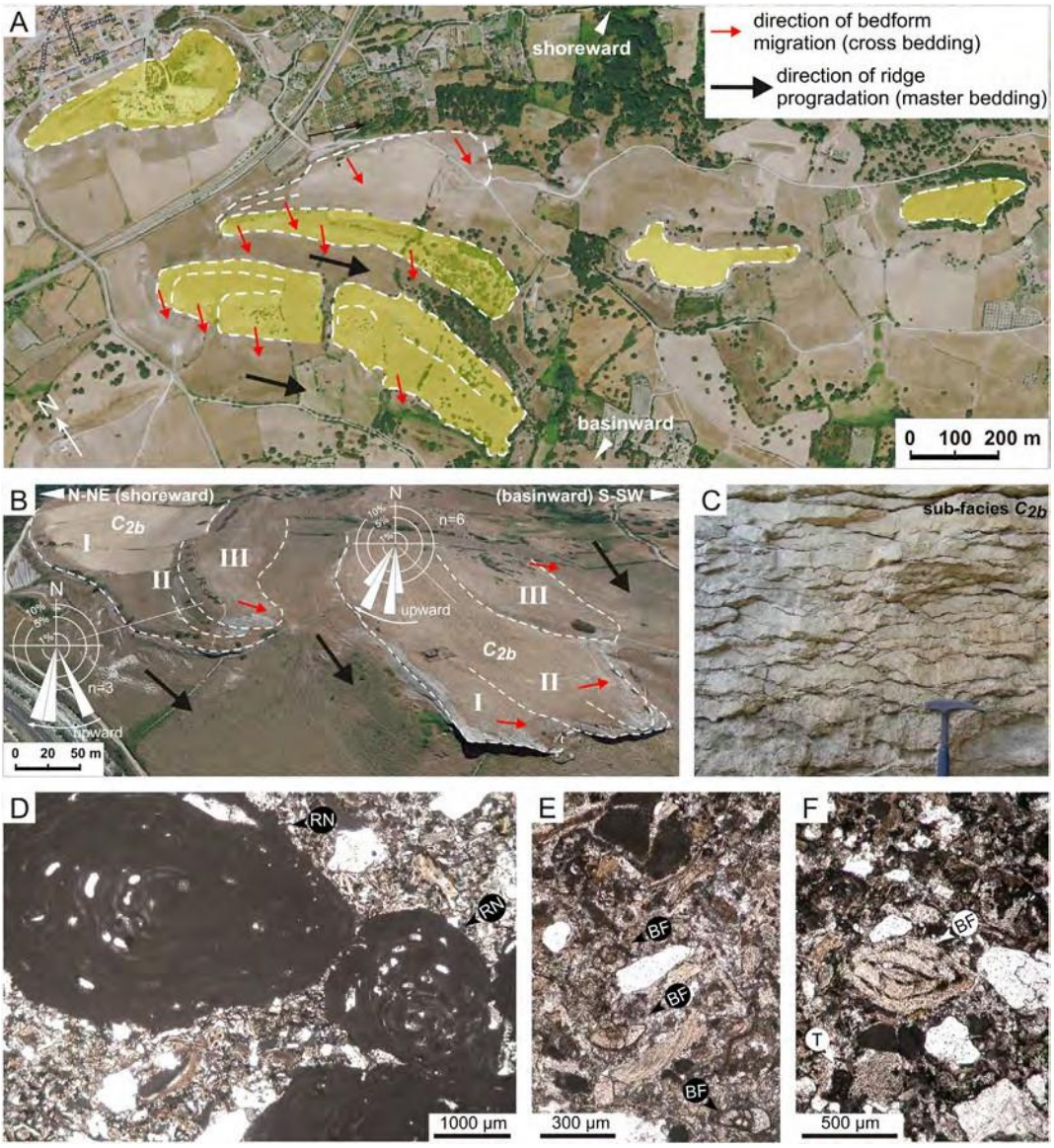
A
shoreward
direction of bedform migration (cross bedding)
direction of ridge progradation (master bedding)
basinward
0 100 200 m
B
N-NE (shoreward)
(basinward) S-SW
C2b
I
II
III
n=3
n=6
upward
0 20 50 m
C
sub-facies C2b
D
RN
1000 µm
E
BF
300 µm
F
BF
T
500 µm

Fig. 13

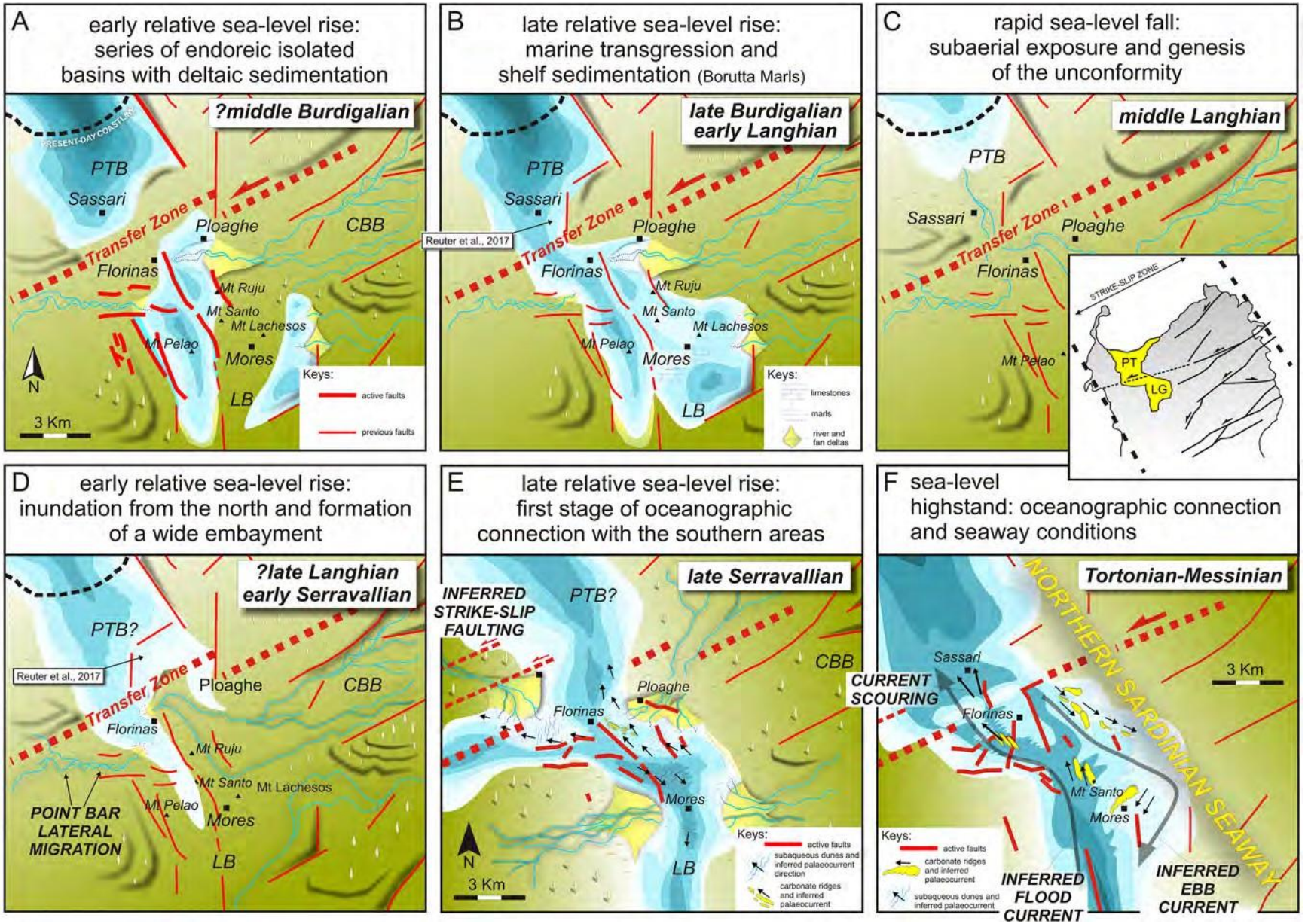
A
early relative sea-level rise:
series of endoreic isolated
basins with deltaic sedimentation
?middle Burdigalian
PRESENT-DAY COASTLINE
PTB
Sassari
Transfer Zone
Ploaghe
CBB
Florinas
Mt Ruju
Mt Santo
Mt Lachesos
Mt Pelao
Mores
LB
N
3 Km
Keys:
active faults
previous faults
B
late relative sea-level rise:
marine transgression and
shelf sedimentation (Borutta Marls)
late Burdigalian
early Langhian
Reuter et al., 2017
limestones
marls
river and
fan deltas
C
rapid sea-level fall:
subaerial exposure and genesis
of the unconformity
middle Langhian
STRIKE-SLIP ZONE
PT
LG
D
early relative sea-level rise:
inundation from the north and formation
of a wide embayment
?late Langhian
early Serravallian
PTB?
POINT BAR
LATERAL
MIGRATION
E
late relative sea-level rise:
first stage of oceanographic
connection with the southern areas
late Serravallian
INFERRED
STRIKE-SLIP
FAULTING
subaqueous dunes and
inferred palaeocurrent
direction
carbonate ridges
and inferred
palaeocurrent
F
sea-level
highstand: oceanographic connection
and seaway conditions
Tortonian-Messinian
NORTHERN SARDINIAN SEAWAY
CURRENT
SCOURING
INFERRED
FLOOD
CURRENT
INFERRED
EBB
CURRENT
subaqueous dunes and
inferred palaeocurrent

Fig. 14

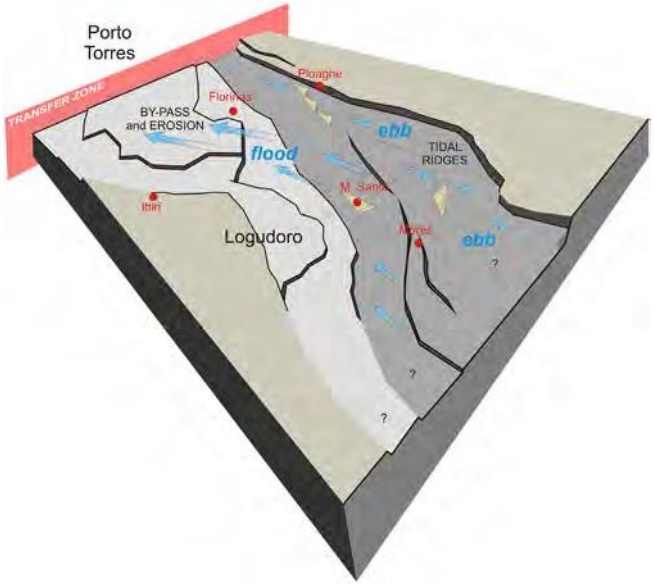
Porto
Torres
TRANSFER ZONE
Florinas
BY-PASS
and EROSION
flood
ebb
TIDAL
RIDGES
M. Santo
Ittiri
Logudoro
ebb
?
?
?

Fig. 15

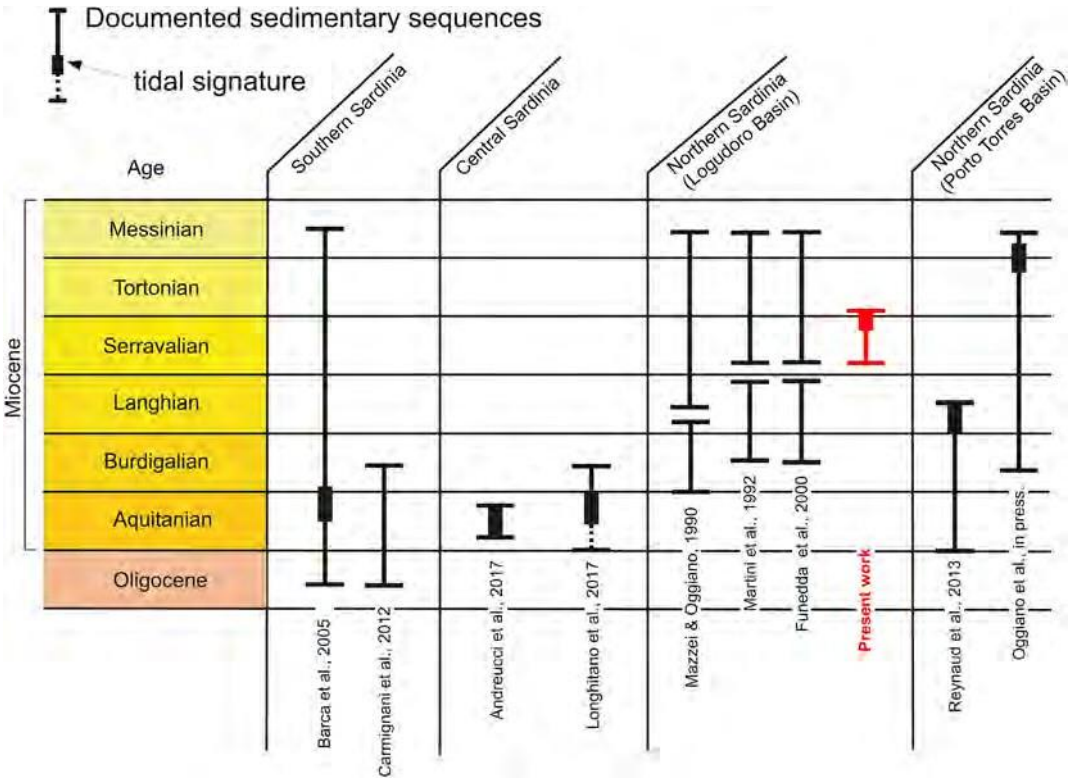
Documented sedimentary sequences
tidal signature
Age
Southern Sardinia
Central Sardinia
Northern Sardinia (Logudoro Basin)
Northern Sardinia (Porto Torres Basin)
Miocene
Messinian
Tortonian
Serravalian
Langhian
Burdigalian
Aquitanian
Oligocene
Barca et al., 2005
Carmignani et al., 2012
Andreucci et al., 2017
Longhitano et al., 2017
Mazzei & Oggiano, 1990
Martini et al., 1992
Funedda et al., 2000
Present work
Reynaud et al., 2013
Oggiano et al., in press.

Fig. 16

Table 1

Facies Ass.	Facies	Sub-Facies	Description			Interpretation	
				Average bed thickness (m)	Fossils, Ichnofacies and Bioturbation Index (BI)	Depositional setting/process	System / Environ.
C	C_2	C_{2b}	Bioclastic grainstone and foramol/rhodalgal floatstone/rudstone. Internally, organised in plane-parallel strat. In dip-oriented sections and clinoforms in strike oriented section. Smaller-scale cross stratified beds show paleocurrents with bipolar directions but oriented at a high angle compared to the orientation of master surfaces.	0.05 - 2	Echinoids, ostreids, rodoliths, pectinids, bryozoans, foraminifera, bivalves, gastropods preserved and in fragments BI = 0 - 1 (*Skolithos, Ophiomorpha*)	Bioclastic ridge core *Processes.* High sedimentation rate related to the lateral migration of ridges and actively accreting bar surface with compound dunes on both sides of the ridges.	CURRENT–DOMINATED SEAWAY
		C_{2a}	Heterolithic deposits, made up of bioclastic mudstone and wackstone and forming plane-parallel stratification.	0.10 - 0.40	Ostreids, rodoliths, bivalves preserved and in fragments BI = 2 - 4 arthropods and worms	Bioclastic ridge margin *Processes.* Deposition in low-energy conditions characterised by the alternation of two processes: the settling from suspension of fine particles (mostly) and downslope movement due to gravity flows.	
	C_1 *tr2*	C_{1b}	Erosional basal boundary characterised by scours associated with shell lags. Matrix- to clast-supported assemblage of coarse-grained particles exhibiting cross-stratified strata sets, including opposite foreset directions.	0.30 -1.5	Bivalve, echinoid and algal fragments BI = 0 - 1 (basal boundary) *(Skolithos, Ophiomorpha)*	Mixed-siliciclastic/bioclastic tidal dunes *Processes.* Bidirectional tractional currents rhythmically changing in strength.	
	tr1	C_{1a}	Heterolithic coarse-grained and fine-grained sandstone, forming medium-scale through cross-stratification, interrupted by discontinuity surfaces. Herringbones and lamina bundles.	0.02 - 0.20	Fragments of shells and echinoids BI = 1 - 3 (*Cruziana*)	Siliciclastic tidal dunes *Processes.* Bidirectional tractional currents affected by ebb-flood and neap-spring tidal cyclicities.	
B	B_2	B_{2b}	Lenticular bioclastic-rich beds with b/s ratio >>1, intercalated with B_{2a}. At thin section scale: grainstone and packstone and algal-rich floatstone/rudstone, containing carbonate matrix and sparite.	1.5 - 5	Echinoids, ostreids, rodoliths, pectinids, bryozoans and foraminifera BI = 0 - 1 (*Skolithos*)	Delta-platform including bioclastic dunes *Processes.* Episodic changes of the main sediment source. Bed-shear stress exerted by along-shore currents.	SUBMERGED DELTAS
		B_{2a}	Moderately- to poorly-sorted medium- to-very coarse sandstone with calcite cement, exhibiting a chaotic textural fabric and with a b/s << 1 and internally including three main orders of sub-horizontal cross stratification.	0.05 - 22	Fragments of pectinids, echinoids BI = 1 - 3 (*Cruziana*)	Delta-platform including siliciclastic dunes *Processes. R*iver-dominated flooding episodes and very rapid deposition. Reworking by traction tidal currents moving in an alongshore direction.	
	B_1	B_{1b}	Structureless or faintly laminated siltstone, forming large-scale cross-stratified foresets. Locally loading and scouring structures.	0.03 - 0.05 (Locally up to 10 m)	Unfosilliferous BI = 0 - 1 (rare vertical traces)	Gravity-dominated and current-influenced delta-slope *Processes.* Gravity-driven turbidity and density flows (mainly), with local shear stress exerted along base surfaces. Sub-facies B_{1b} records settling of fine sediment from suspensions or stages of delta abandonment due to delta-lobe switching processes.	
		B_{1a}	Coarse sandstone, exhibiting sub-angular to rounded clasts, and pebbles, forming large-scale cross-stratified foresets. Single strata show erosional bases, either normal and reverse grading, or display bi-partite grain-size zones.	0.05 - 0.10			
A	A_3	-	Conglomerates, coarse-grained sandstone, and siltstone in places, organised into tabular to lenticular beds, normally graded and including cross stratification with foresets separated by internal erosional shallow scours.	0.20 - 1	Unfosilliferous BI = 0	Ephemeral streams *Processes.* Lateral migration of bars in low energetic conditions.	RIVERINE BRAID PLAIN
	A_2	A_{2b}	Greyish siltstone, subordinate fine-grained sandstone, lenticular intercalations of sub-rounded polygenic pebbles and cobbles at the base of beds. Indistinct internal cross lamination.	0.40 - 2	Unfosilliferous BI = 0	Inter-channel flood plains *Processes.* Sedimentation from suspension during floods. Local deposition of gravel (closer to river channels).	
		A_{2a}	Normally graded tabular beds with erosional bases, forming a fining-upward succession, made up of coarse-grained sandstone and subordinate siltstone, including rounded granules, forming lamination or being scattered. Internally, indistinct low-angle cross lamination.		Unfosilliferous BI = 1 (*Glossifungites*)	Crevasse splays *Processes.* Basal erosion and deposition of gravel and progressive settling of the suspended load as the flow loses velocity. High-density flows, responsible for the generation of local traction carpets.	
	A_1	A_{1b}	Amalgamated, plain-parallel laminated sets made up of poorly sorted, coarse- to very coarse-grained arkose, with erosional bases and normally graded.	1 - 3	Unfosilliferous BI = 0	Braided channels *Processes*. Erosion followed by deposition by tractive currents with decreasing velocity and shallowing due to the progressive filling of the channels	
		A_{1a}	Cross-laminated sets made up of polymictic, pebbly sandstone and conglomerate, with angular to sub-rounded elements, forming vertically stacked cosets.			Point bars accreting laterally *Processes.* Deposition exerted by tractive currents, producing bar lateral accretion	